AN ABSTRACT OF THE THESIS OF

Elena M. Nes for the degree of Master of Science in Radiation Health Physics presented on May 28, 2002.

Title: Comparison Between AAPM's TG-21 and TG-51 Clinical Reference Protocols for High-Energy Photon and Electron Beams.

Abstract approved: Redacted for Privacy

Kathryn A. Higley and Steven R. Reese

In radiation therapy it is very important to accurately measure the amount of radiation delivered. The effectiveness of the treatment depends on delivering the dose with an accuracy of 5% or better. The dosimetry in different clinics must also be consistent. For these reasons national and international calibration protocols have been developed. In the US, the American Association of Physicists in Medicine (AAPM) has published several national dosimetry protocols for the calibration of high-energy photon and electron beams.

In this study the absorbed dose-to-water determined according to TG-21 and TG-51 protocols, developed by Task Group 21 and Task Group 51 of the Radiation Therapy of AAPM, are compared. The older protocol, TG-21, is based on exposure calibrated ionization chambers using a ^{60}Co beam. Many standards laboratories have started to replace exposure standards with those involving absorbed dose-to-water. The new protocol, TG-51, is based on absorbed dose-to-water calibrated ionization chambers using a ^{60}Co beam. Also, there are some differences between the beam quality specifiers and data proposed by the two protocols.

A comparison between TG-21 and TG-51 protocols was done by determining the radiation dose rate at a designated distance for 6 and 18 MV photon beams, and 16 and 20 MeV electron beams, generated by Clinac a 2100 C linear accelerator. The cylindrical ionization chambers used in this study were Capintec PR-06G and PR-05.

The results of the study show a discrepancy between the absorbed dose-to-water determined according to TG-21 and TG-51 protocols of about 1.4% and 1.7% for 6 and 18 MV photon beams, respectively. Absorbed dose-to-water determined according to TG-21 and TG-51 protocols for 16 MeV energy electron beams agree within 1.8%, while the ones of 20 MeV energy beams agree to within 2.4%. The change from exposure to absorbed dose-to-water calibrated ionization chambers has the largest impact on the differences between TG-21 and TG-51 absorbed dose-to-water, while the change in beam quality specifier and stopping power ratios have only a very small effect on these differences.

The TG-51 protocol is very simple, minimizing the chance of mistakes, because it starts with absorbed dose-to-water calibration, while the TG-21 is very complex, starting with the calibration for exposure, which is different from the absorbed dose-to-water, the clinical quantity of interest. The TG-51 protocol allows the determination of a more accurate absorbed dose in a ^{60}Co beam than the TG-21 protocol since it uses an absorbed dose-to-water calibration factor directly measured, while the exposure based dosimetry system is dependent on external physical data which are not measured in clinics.

Comparison Between AAPM's TG-21 and TG-51 Clinical Reference Protocols for High-Energy Photon and Electron Beams

By

Elena M. Nes

A THESIS

submitted to

Oregon State University

in partial fulfillment of
the requirements for the
degree of

Master of Science

Presented May 28, 2002

Commencement June 2003

Master of Science thesis of Elena M. Nes, presented on May 28, 2002.

APPROVED:

Redacted for Privacy

Co-Major Professor, representing Radiation Health Physics

Redacted for Privacy

Co-Major Professor, representing Radiation Health Physics

Redacted for Privacy

Head of Department of Nuclear Engineering

Redacted for Privacy

Dean of Graduate School

I understand that my thesis will become part of the permanent collection of Oregon State University libraries. My signature below authorizes release of my thesis to any reader upon request.

Redacted for Privacy

Elena M. Nes, Author

ACKNOWLEDGMENTS

First of all, I would like to thank my co-major professor, Dr. Steven R. Reese, whom was the driving factor to the successful completion of this thesis. I am grateful for his support and understanding and I greatly appreciate his patience with me during the thesis writing stage. His expertise and guidance added considerably to my graduate experience. Without his encouragement I wouldn't have considered continuing studies. I doubt that I will ever be able to express my appreciation entirely, but I owe him my eternal thankfulness.

I would like to express my deepest gratitude to Dr. Kathryn A. Higley, my co-major professor, who carefully guided me throughout the pursuit of my Master degree at OSU. She is one of the best professors I ever had, always friendly and approachable through my time in the department. Her ideas and suggestions have been invaluable to this thesis. It was a privilege for me to have her as major adviser.

I am particularly thankful to Dr. Todd S. Palmer for the all the support that have given me throughout my entire graduate program. His feedback on earlier drafts made a much improved final product.

I must give immense thanks to Mr. Thomas M. Potts, MS, DABR, for taking time out from his busy schedule to offer me the opportunity to use the Corvallis Cancer Center linear accelerator at acquiring the experimental data used in this thesis. Without his expertise none of this work would have been possible. Thank you for all the support without which I couldn't consider a career in Medical Physics.

Also, I am grateful to Dr. Gobeli, my Graduate Council Representative for the advice and time given me.

I would also like to thank to the faculty and staff at the OSU Radiation Center.

Finally I thank my daughter, Georgiana for her love and understanding.

TABLE OF CONTENTS

TABLE OF CONTENTS (CONTINUED)

LIST OF FIGURES

LIST OF FIGURES (CONTINUED)

LIST OF TABLES

LIST OF APPENDICES

LIST OF APPENDICES (CONTINUED)

COMPARISON BETWEEN AAPM'S TG-21 AND TG-51 CLINICAL REFERENCE PROTOCOLS FOR HIGH-ENERGY PHOTON AND ELECTRON BEAMS

1. INTRODUCTION TO RADIATION THERAPY

1.1. INTRODUCTION

Therapeutic radiology is a field devoted to the treatment of malignant diseases. The field was born not long after the discovery of x-rays by Wilhelm Roentgen in 1895. The first therapeutic use of x-rays was in 1896 when a German physician, Dr. Freund, showed that he could cause the disappearance of a hairy mole following x-ray treatments (Pusey 1900).

Radiotherapy along with surgery and chemotherapy form the backbone of modern cancer management. It is estimated that about 70% of all cancer patients benefit from radiation treatments at some point during their care (Wambersie et al. 1996). Radiation therapy is useful in cases where surgical removal of the cancer is not possible or when surgery might debilitate the patient. Radiotherapy can also be used following surgery to destroy any cancer cells that were not removed by surgery, or prior to surgery to shrink a previously inoperable tumor to a manageable size. If a cure is not possible, radiation helps relieve symptoms of advanced cancer such as bleeding or pain. Like all forms of cancer treatment, radiation therapy can have side effects. Possible side effects of treatment with radiation include increased risk for future cancer, vascular damage, temporary or permanent loss of hair in the area being treated, skin irritation, temporary change in skin color in the treated area, and tiredness. Other side effects are largely dependent on the area of the body that is treated.

1.2. TYPES OF RADIATION USED IN RADIOTHERAPY

The radiation used in radiotherapy is ionizing radiation, having enough energy to remove an orbital electron from an atom, resulting in an ion-pair. This radiation can have an electromagnetic form such as high-energy photons or particulate form such as electrons, and can be classified as directly or indirectly ionizing. Electrons are directly ionizing, delivering their energy to matter directly, through many small Coulomb-force interactions along the particle's track. Photons are indirectly ionizing since they first transfer their energy to electrons in the matter through which they pass and the resulting electrons in turn deliver the energy as charged particles. The deposition of energy in matter by indirectly ionizing radiation is thus a two-step process.

Ionizing photons interact with the atoms of a tissue to produce electrons by three important mechanisms: the photoelectric effect, the Compton effect, and pair production.

In the photoelectric effect, an incoming photon undergoes a collision with a tightly bound electron (K, L, or M shell) of an atom of the absorbing material. As a result of the collision the photon gives up all of its energy to the electron that is ejected. The energy of the ejected electron is equal to the energy of the photon minus the binding energy of the electron. The process is more likely to occur if the photon energy is just greater than the binding energy of the electron. The probability of photoelectric absorption depends on the energy E of the incoming photon, and on atomic number Z of the tissue, being proportional approximately with $\frac{Z^3}{E^3}$. The lower the energy and the higher the atomic number, the more likely a photoelectric effect will take place (Johns et al. 1983). For photoelectric collisions in tissue, one can assume that all the energy is locally absorbed. In radiotherapy high-energy photons in the megavolt range are used, so the photoelectric effect is negligible.

The Compton effect is the most important photon-tissue interaction for the treatment of cancer. In this case, photons collide with "free electrons," i.e. electrons that are not tightly bound to the atom. Unlike the photoelectric effect, both the photons and electrons are scattered. The photons can then continue to undergo additional interactions, though with a lower energy. The electrons are mainly forward-directed (Attix 1986) and

ionize matter as they continuously slow down. The probability of a photon interacting in a Compton collision with a free electron may be evaluated by the Klein-Nishina formula (Johns et al. 1983) and is inversely proportional to the energy of the incoming photon and independent of the atomic number of the material. As a consequence, the absorbed dose is about the same in soft tissue, muscle and bone. When low energy photons interact in a Compton process, very little energy is transferred to the medium and most of the energy is scattered, so many interactions are required to absorb the beam. If the energy of the photon is large, 10 to 100 MeV, most of the energy is transferred to the recoil electron and very little is scattered.

When the energy of the incident photon is greater than 1.02 MeV the photon may be absorbed through the mechanism of pair production. In pair production a photon interacts with the nucleus of an atom. The photon gives up its energy to the nucleus and, in the process, creates a pair of positively and negatively charged particles (positron and electron respectively). The positron loses energy through successive ionizations until it combines with a free electron. This generates two 0.511 MeV photons that are emitted in opposite directions. The probability of pair production is proportional to the logarithm of the energy of the incoming photon and to the atomic number of the material (Johns et al. 1983). This interaction does occur to some extent in routine radiation treatment with high-energy photon beams.

The importance of the three processes described above is summarized in Table1.1 (values for soft tissue).

Table 1.1. Dominant photon interaction processes and the corresponding photon energy ranges for soft tissue (Johns et al. 1983)

Energy	Process
Up to 50 keV	Photoelectric is important.
60 keV to 90 keV	Photoelectric and Compton are both important.
200 keV to 2 MeV	Compton absorption alone is present.
5 MeV to 10 MeV	Pair production begins to be important.
50 MeV to 100 MeV	Pair production is the most important.

In addition to photons, electron beams are also used in radiotherapy. As electrons travel through a medium, they interact with atoms by a variety of processes due to a Coulomb force field. From the point of view of radiation therapy the most important processes are inelastic collisions with atomic electrons (ionizations and excitations) and inelastic collisions with nuclei (bremsstrahlung).

Due to the relatively small mass of the electron, relativistic effects are important even at low energies. Since electrons collide with other electrons, they may lose in a single collision a large fraction of their kinetic energy and suffer marked changes in direction, leading to tortuous paths. The energy loss by an electron of certain energy in producing ionization in the absorbing medium per unit path length is called stopping power (S). By dividing the stopping power by the density of the medium ρ one obtains the mass stopping power $\left(\frac{S}{\rho}\right)$ measured in $\frac{MeVcm^2}{g}$. In dense media the interactions between the passing charged particle and distant atoms are diminished due to the screening effect of dipole-distorted atoms near the particle track. This is called the "polarization effect" and it is taken into account in Bethe-Moller formula for $\left(\frac{S}{\rho}\right)$ by including a polarization correction term, which is a function of the composition and density of the stopping medium (Attix 1986). Due to polarization, a high-energy electron loses more energy per gram per square centimeter in a gas than in a more dense medium as a result of appreciable polarization of the condensed medium.

In the case of an electron spectrum a spectrum-weighted mean mass stopping power $\left(\frac{\bar{S}}{\rho}\right)$ is used:

$$\left(\frac{\bar{S}}{\rho}\right) = \frac{\int_0^E \phi(E)\left(\frac{S}{\rho}\right)(E)dE}{\int_0^E \phi(E)dE} \qquad (1\text{-}1)$$

where $\phi(E)$ is the distribution of electron fluence in energy (Johns et al. 1983). The electrons can be characterized by a range, beyond which there are no particles.

In interaction with the electric field of a nucleus electrons may be decelerated rapidly, radiating energy as bremsstrahlung. The energy loss by radiation increases directly with the atomic number of material and with the energy of the electron. The bremsstrahlung has a continuous spectrum of energies.

1.3. FACTORS LEADING TO CANCER

Cancer is a group of diseases characterized by uncontrolled growth and spread of abnormal cells. Exceeded only by heart disease, cancer is the second leading cause of death in the USA. According to the American Cancer Society, about 1,284,900 new cases are expected to be diagnosed in 2002 (ACS 2001).

Normal cells divide and replace themselves in an orderly process. Any injury to a cell may effect the structure of DNA and thus the cell cycle, so as a major defense against environmental damage to DNA, cells have evolved DNA repair mechanisms.

Cancer can occur in cells with deficient DNA repair mechanisms. There are necessary mutations of DNA sequence in several genes that control the cell cycle before a cell can become cancerous. The accumulation of these mutations requires time, so cancer becomes more common as one gets older. In some cancers, the rate of division is fast, in and in others it is slow, but in all cancers the cells never stop dividing, multiplying and forming clumps of tissue called tumors. No matter how many trillions of cells are present in a tumor, they are all descended from a single ancestral cell.

Cancer cells almost always include mutations of the DNA sequence in genes controlling the cell division as growth-stimulating and growth-inhibiting genes. The defective growth-stimulating genes leading to cancer are called oncogenes. Ras is a growth-stimulating gene found in normal cells, which acts as a switch. When receptors on the cell surface are stimulated (by a hormone, for example), Ras is switched on, transmitting signals that tell the cell to grow. If the cell-surface receptor is not stimulated, Ras is not activated and the pathway that results in cell growth is not initiated. The oncogenic form of Ras is always active telling the cell to grow regardless of whether receptors on the cell surface are activated or not (Campbell et al. 1999).

Changes in growth-inhibiting genes also contribute to cancer. Such genes are called tumor-suppressor genes because they prevent uncontrolled cell growth, killing cells with oncogenes. Any mutation that decreases the normal activity of a tumor-suppressor gene may contribute to the onset of cancer, in effect stimulating growth through the absence of suppression. The protein products of tumor-suppressor genes have various functions. For instance, some tumor-suppressor proteins repair damaged DNA, a function that prevents the cell from accumulating cancer-causing mutations. When DNA damage is irreparable, they trigger cell death by a process called apoptosis. Others proteins control the adhesion of cells to each other or to an extracellular matrix. Proper cell anchorage is crucial in normal tissues and is often absent in cancers, allowing the cancer to spread into nearby tissues. An example of a tumor-suppressor gene is p53, which is often called "the guardian angel of the genome". Mutation of the p53 gene is probably the most significant genetic change characterizing the transformation of cells from normalcy to malignancy (Campbell et al. 1999).

Other mutated genes in cancer cells are those that maintain telomeres, the chromosome tips. Normal cells lose a portion of their chromosome tips at each mitosis. This establishes a limit to the number of times they can divide before the chromosome becomes too short and in this way limits the life span of any cell lineage. Telomere shortening can be avoided by telomerase, an enzyme that extends the telomeres. Most normal cells do not contain telomerase. Malignant cells have the ability to express telomerase and in this way gain immortality (Campbell et al. 1999).

1.4. DELIVERY OF RADIOTHERAPY

Radiation therapy works to destroy cancer cells by two mechanisms: first, immediate cellular death when the cell may no longer perform its function due to internal ionization, and second, mitotic cell death when the cell can no longer reproduce because of the damage of its DNA (Ross 1999). Once the DNA has been damaged by ionizing radiation, the cancer cells are not able to divide and grow, causing the tumor to shrink. Radiation therapy treatments are designed to destroy cancer cells while limiting the amount

of normal tissue exposed and injured by the rays. Special shields may be used to protect parts of the body that do not require treatment. Despite these protective measures, some normal cells are effected by radiation therapy. However, these healthy cells are generally able to recover more fully from the effects of radiation, since they are typically much better at using the body's natural repair mechanisms to correct the DNA damage.

Radiation therapy can be given in one of two forms: internal and external. Internal radiation therapy (brachytherapy) places the source of the high-energy rays inside the body as close as possible to the cancer cells. This delivers continuously a very intense radiation dose to a small area of the body and limits the dose to normal tissue. Internal radiation therapy allows the delivery of a higher total dose of radiation in a shorter time than is possible with external treatments. The radioactive substances typically used include radium, cesium, iodine, and phosphorus, and they may be implanted for only a short time or permanently left in place. Patients with radiation implants need to be isolated from visitors so as not to expose them to radiation. Internal radiotherapy is frequently used for cancers of the tongue, uterus, and cervix.

External-beam radiotherapy uses linear accelerators that direct high-energy x-rays at the cancer and surrounding normal tissues. External radiation is delivered in fractions, either daily or several times a week, until the total dose needed to kill the tumor has been reached. It has been shown that one single large dose of radiation produces profound effects on normal tissues limiting the clinical utility of this treatment. Fractionation was developed as a means of sparing normal tissue while still effectively treating tumors. The efficiency of fractionation can be explained by appealing to the four R's of radiobiology: repair of sublethal damage, repopulation, reassortment of cells within the cell cycle, and reoxygenation (Hall 1994).

Malignant and normal cells differ little in their response to ionizing radiation. Both cell types are more sensitive to radiation during the mitotic (division) phase and less so during the DNA synthesis phase. Fractionating the total dose allows the healthy tissue time to repair between treatments, while tumor cells, being less proficient at DNA repair, are not as able to heal themselves as are normal cells. Waiting between doses also allows time for repopulating. Both normal and malignant cells divide between doses of radiation and thus increase their apparent survival. Reassortment of cells also plays an important role

in tumor control. When a large dose of radiation is given, most surviving cancer cells are in the resistant phase of the cell cycle DNA synthesis phase. A second dose of radiation would not be as effective because these cells are relatively resistant. However, if time is allowed, the cancer cells reassort themselves into more sensitive phases of the cell cycle and a second radiation dose at this point would again be effective. Fractionation also allows cancer cells to become better oxygenated. Only tumors have areas of relative hypoxia (oxygen depletion) because they do not exhibit density dependent inhibition. They pile up on each other, so some of them are at a distance greater than the distance to which oxygen from a capillary can diffuse. These oxygen-starved areas are relatively radioresistant, oxygen enhances the effects of radiation. When sufficient doses of radiation are given to kill the oxygenated cancer cells, the oxygen-deprived cells redistribute into more oxygenated regions, thus becoming more sensitive to radiation. However, normal tissues do not have these areas of hypoxia so fractionation would tend to spare them.

Both normal and malignant tissues have sigmoid dose-response relationships: a certain radiation dose is necessary before a response is observed. The doses that are needed to control a malignant tumor are often of the same order of magnitude as the tolerance doses for normal tissues. However, a tumor is more sensitive than the normal tissues. At the doses that are typically delivered in radiation therapy for tumor control, the dose response curves for normal and tumor tissues are steep. For small dose decrements the tumor response is strongly diminished, while for small dose increments the damage produced by radiation to normal tissues is dramatically increased (Figure 1.1). For these reasons accurate dosimetry is needed. The accuracy in delivery of an absorbed dose to a target volume, recommended by the International Commission on Radiation Units and Measurements (ICRU), is about $\pm$ 5% (Wambersie 1996).

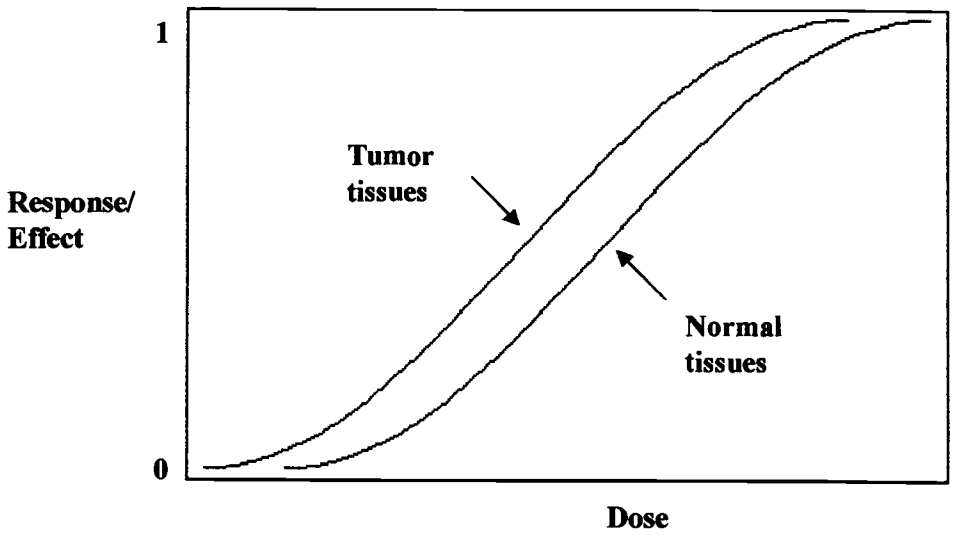

Figure 1.1. Idealized dose response curves for tumor and normal tissues

High-energy photon beams are used in over 90% of external-beam radiation therapy treatments (Mackie 1997). X-rays and gamma rays enter biological material and their energy is converted into thermal energy, which breaks chemical bonds, leading to cell death. The maximum dose occurs below the skin surface, fact accounting for the skin sparing properties of high-energy photons. They are used for treating deep-seated tumors.

Radiotherapy can also use electron beams. They are used for treating superficial tumors up to a depth of about 5 cm because they interact as soon as they enter the patient and they lose energy in the patient as they eventually slow down coming to rest. The range of the electron beam depends on the energy, so that low energy electron beams do not penetrate the skin, while higher energy electron beams penetrate tissues to a moderate extent and then their energy rapidly drops off. This becomes important when irradiating certain neck tumors. High-energy electron beams are able to reach the tumors fairly well but then their energy drops off quickly so that the spinal cord is spared of radiation exposure.

Electron absorption in human tissue is greatly influenced by the presence of air cavities and bone. The dose is increased when the high-energy electron beam passes through an air space and is reduced when the beam passes through bone. This can be

explained by the "polarization effect" (Attix 1986) presented in Section 1.2. Relating the absorbed dose in the gas to that in the solid surrounding medium (Brag-Gray cavity theory) requires knowledge of the stopping powers which are influenced by the polarization effect in the solid. This polarization effect is important for radiotherapy, particularly in ionization chamber measurements for electron and photon beams above 2 MeV.

The mean stopping powers and mass attenuation coefficients used in the determination of absorbed dose are functions of the spectrum of electrons at the point of measurement. This spectrum, in turn, is a function of the energy of the incident x-rays or electrons. Thus for correct determination of these parameters one has to determine with accuracy the beam quality, Q. An ideal way to describe the quality of a beam is to specify its spectral distribution. However, these spectral distributions are difficult to measure. In radiotherapy, the quality of a photon beam is typically characterized in terms of its ability to penetrate materials and an electron beam is typically characterized by electron range.

1.5. MEDICAL LINEAR ACCELERATORS

Medical linear accelerators are the key systems used for delivering radiotherapy treatments (Johns et al. 1983). The accelerator consists of four major components: an electronics cabinet (called a "stand") housing a microwave energy generating source, a rotating gantry containing the accelerator structure that rotates around the patient, an adjustable treatment couch and operating electronics (Figure 1.2). The linear accelerator is capable of rotating around a patient lying on a treatment couch to provide maximum dose to a point at the center of rotation and less dose at all radial sites. This allows the delivery of high doses of radiation to the tumor while reducing the dose to the normal surrounding tissues. Accelerators are located within specially constructed concrete treatment rooms to provide X-ray shielding.

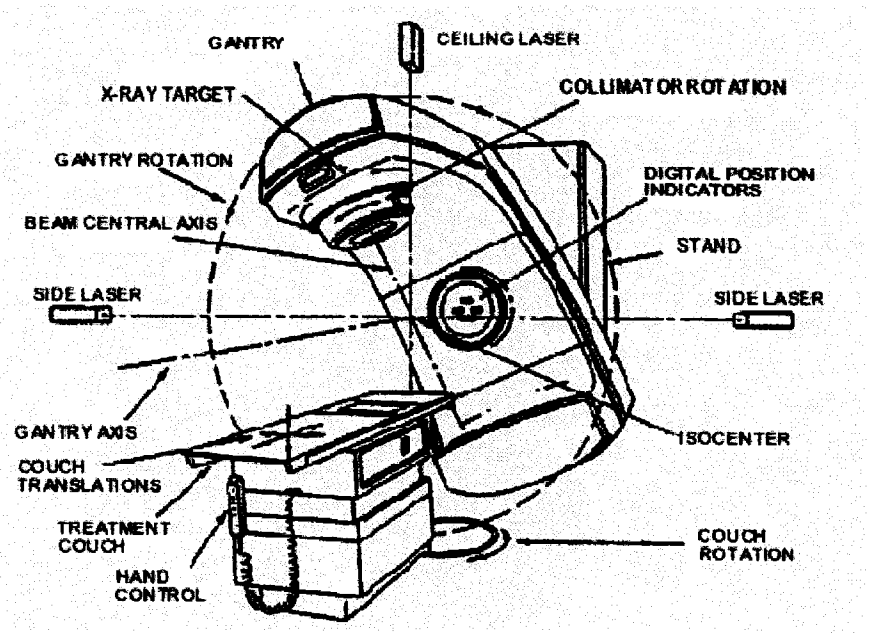

Figure 1.2. Schematic diagram of a typical medical linear accelerator
(Courtesy of Dr.Rock Mackie, Department of Medical Physics, University of Wisconsin)

Microwave energy is used to accelerate electrons to nearly the speed of light. They attain this velocity in a short distance, typically one meter or less. As high-energy electrons emerge from the exit window of the accelerator structure, they are in the form of a pencil beam about 3 mm in diameter. The high-energy electron beam itself can be used for treating superficial tumors, or it can be made to strike a target to produce x-rays, which can be used further for treating deep-seated tumors.

When a photon beam is desired, the electrons are directed towards a copper target. Occasionally the electrons will closely approach the nuclei of the target atoms and suffer an energy loss. The sudden deceleration of the electrons gives rise to bremsstrahlung x-rays. The bremsstrahlung x-ray spectrum is continuous with the maximum energy equal to the incident electron energy. The average photon energy of the beam is approximately one-third of the maximum energy. The target has to be thick enough to absorb most of the incident electrons, and due to the amount of heat produced, it is normally water-cooled. Because high-energy electrons are used to produce x-rays, photons are emitted primarily in

the forward direction of the electrons, giving a circular distribution on the patient's skin as shown in Figure 1.3(a) A flattening filter is inserted in the beam in order to make the beam intensity uniform across the field (Figure 1.3(b)). The filter is a circular piece of metal, thicker in the center than at the edge (Khan 1984). For large fields, the beam is often contaminated with low energy electrons, which can be removed by an electron filter.

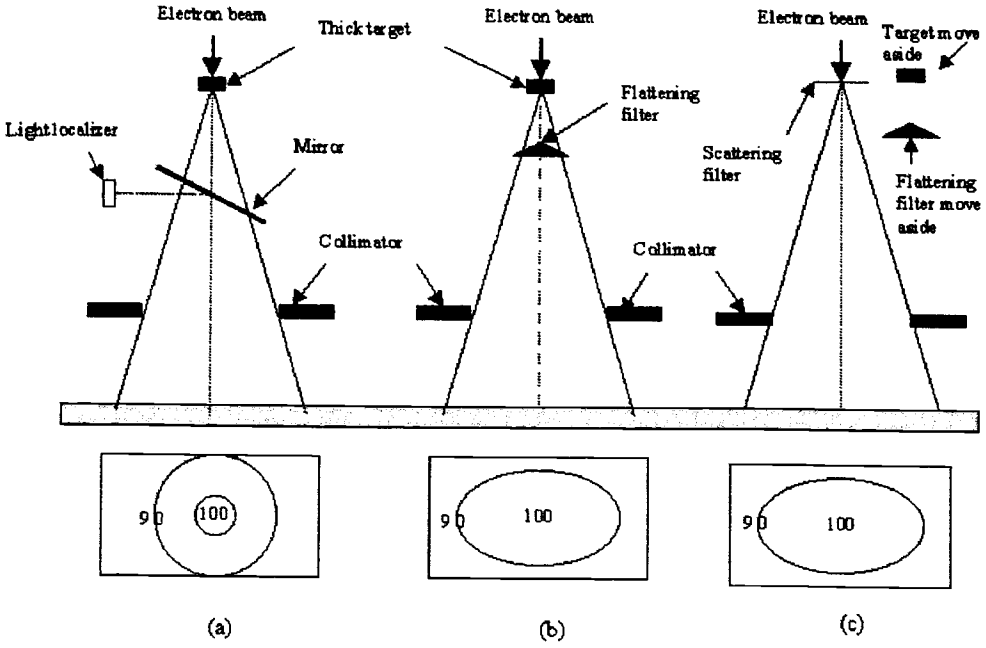

Figure 1.3. Schematic diagram describing the components of the head of a linear accelerator. (a) X-ray therapy mode - Non-uniform dose distribution; (b) X-ray therapy mode - Uniform field obtained with flattering filter; (c) Electron therapy mode

A wedge filter can be used to optimize the dose distribution if the treatment surface is curved or irregular in shape. It is usually made of a dense material, such as lead or steel. In general, the wedge filter alters the beam quality by preferentially attenuating lower energy photons (beam hardening).

In order to produce an electron beam, the target is moved away from the path of the beam and the accelerated electrons are directed at an electron scattering foil as shown in Figure 1.3(c). This spreads the beam and produces a uniform fluence across the

treatment field. The scattering foil is a thin metallic foil usually made of lead. The thickness of the foil is such that electrons are scattered and bremsstrahlung contamination of the electron beam is minimized (Johns et al. 1983).

The electron beam is designated by the term million electron volts (MeV) because it is almost monoenergetic before incidence on the patient surface. The x-ray beam, on the other hand, is heterogeneous in energy and is designated by megavolts (MV) as if the beam was produced by applying that voltage across a x-ray tube.

For the radiation beam to conform to a certain size, high atomic number collimators are installed in the machine. The collimator is a mechanism that controls the dimensions of the primary radiation beam. Types of collimators are cones, diaphragms, and variable-aperture beam-limiting devices. The field size represents the projection of the distal end of the collimator on a plane perpendicular to the beam axis laid at a reference distance, such as the source-surface distance (SSD) or source-axis distance (SAD) (Figure 1.4). The first term represents the distance from the source of the treatment machine to the surface of the patient, and the latter is the distance from the source to isocenter. The isocenter is the intersection of the axis of rotation of the gantry and the axis of rotation of the collimator for the treatment unit. It is the point in space at a specified distance from the source or target that the gantry rotates around. Each isocentric machine has its own SAD, which for most modern linear accelerators it is 100 cm. When the gantry rotates around the patient, the SSD will continuously change. However, the source and isocenter are at a fixed distance and therefore the SAD does not change. Field size changes with distance from the source of radiation because of divergence (Johns et al. 1983).

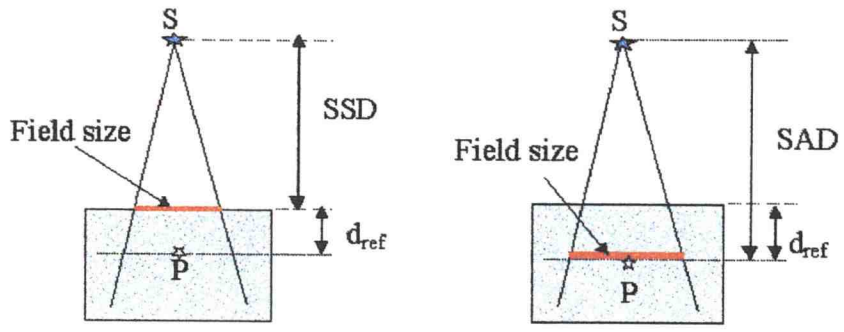

Figure 1.4. Diagram to illustrate the meaning of SSD, SAD and field size

For the purpose of making visible to the clinician the irradiated area, a light and mirror combination is used, the light field simulating the radiation field defined by the collimator.

The normal tissue that remains in the treatment field may be shielded by placing in the beam blocks constructed of a combination of bismuth, tin, cadmium, and lead, named Lipowitz' metal. In this way the dose can be delivered to the tumor at a higher level than if the normal structures were in the field. These individually constructed blocks are used in both x-ray and electron treatments. Recently, multileaf collimators mounted inside the gantry have been developed to provide computerized, customized blocking instead of having to physically construct a new block for each field.

The Clinac 2100 C linear accelerator manufactured by Varian Medical Systems features a patented beam generation system, along with computer-controlled setup and beam delivery (Varian 1999). The Clinac 2100 C is digital as opposed to older systems, which are analog. Another advantage of the Clinac 2100 C is its multileaf collimator (MLC) that can be positioned for convenient setup of asymmetric fields. The linear accelerator and multileaf collimator work simultaneously to deliver radiation therapy that is both more effective and safer for patients. The linear accelerator delivers high-energy x-rays and electron beams to tumors, while the MLC, molds the x-ray field to the exact specifications of the tumor with pinpoint accuracy. Because the field of radiation is shaped to affect the tumor only, surrounding healthy cells are spared. Due to increased safety and

decreased radiation exposure of normal tissues, tumors can be treated with higher, more effective doses (Figure 1.5).

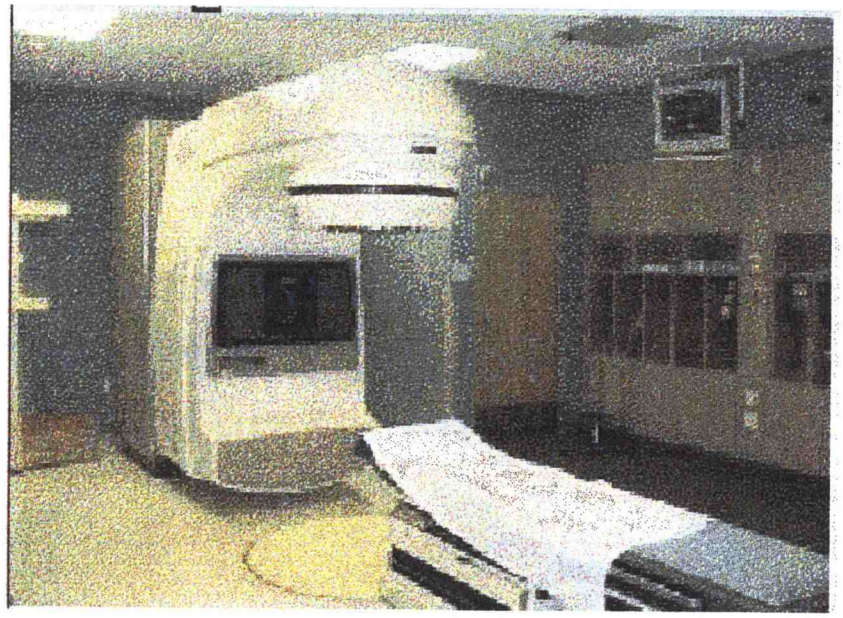

Figure 1.5. Varian Clinac 2100 C linear accelerator

1.6. RADIATION DOSIMETRY AND THEORY

Three quantities play a central role in clinical dosimetry: exposure, kerma, and absorbed dose (Johns et al. 1983).

Exposure is defined as the absolute value of the total charge of the ions of one sign produced in dry air when all of the electrons liberated by the photons in the mass of air are completely stopped within it. Exposure is a measure of the ability of the radiation to ionize air. The System International (SI) unit for exposure is C/kg, but the old unit, the roentgen (1 R= 2.58×10^{-4} C/kg) is still used. The definition refers to all electrons set in motion by photons in the volume of air with mass m. The exposure definition suffers from two limitations. The first is that it is only defined for photons interacting in air. The second is

that the quantity becomes ill-defined as photon energies become higher than 3 MV because the range of electrons slowing down becomes so large that is difficult to truly measure exposure.

These problems are both overcome by introducing the quantity kerma, which is the Kinetic Energy Released per unit Mass and is measured in J/kg or Gray (Gy). For photon beams the kinetic energy released is the kinetic energy transferred to electrons in the material. The quantity must always be defined with respect to the specific material in which the interactions are taking place (e.g. air-kerma, water-kerma). For kerma it does not matter whether the charged particles slow-down inside the volume or not.

The absorbed dose D_m to a material is the energy absorbed in a small mass of material. For a volume large compared to the tracklength, the kerma and absorbed dose are virtually identical. Absorbed dose has the further advantage that it is direct measurable (e.g. by calorimetry) whereas kerma can not be directly measured. The basic unit of radiation absorbed dose is also J/kg or Gray (Gy). The purpose of radiation dosimetry is to establish the absorbed dose.

Estimates of absorbed dose in soft tissue are easily obtained through the use of dosimeters. Ionization chambers are the most widely used type of dosimeter for precise measurements because of their long term stability, high precision and direct readout. As shown in Figure 1.6, an ionization chamber consists of a thin wall, a volume of air with a voltage applied between the wall and an electrode to collect the charged produced in the air by ionizing radiation. The inside of the chamber represents the negative electrode and is coated with a conducting material (e.g. carbon). The central rod represents the positive electrode and is usually made of aluminum.

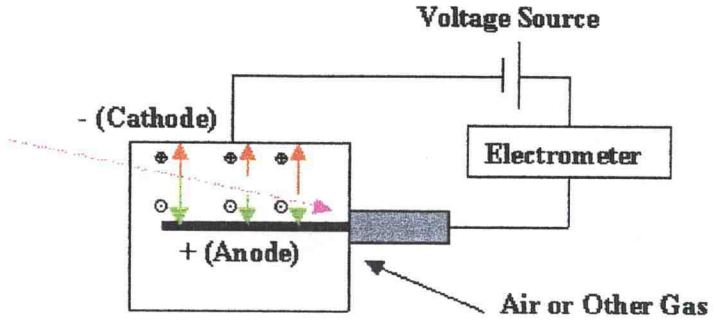

Figure 1.6. Schematic of an ionization chamber.

In the absence of ionizing radiation the gas is an insulator and no electrical current flows between the electrodes. Ion pairs are produced as ionizing radiation interacts in a medium. These ion pairs produce additional ionization as they dissipate their energy by interacting with nearby atoms. Essentially all the ionization in the air cavity is generated by electrons, which enter from the surrounding material.

As the gas is ionized, a small amount of current is established as electrons and ionized atoms migrate to the positive and negative electrodes, respectively. Measurement of this "ionization current" is the basic principle of the ion chamber. Collected charge of either sign can be measured by an electrometer. Some of the electrons, generated by gas ionization, produce ionization outside the collecting volume. However, the collecting volume may be chosen so that the ionization produced outside the volume by electrons produced inside it is balanced by ionization produced inside the volume by electrons originating outside (Figure 1.7). This condition, known as charged particle equilibrium (CPE), results in the collection of a charge inside the volume of the chamber equal to the total ionization (Johns et al. 1983).

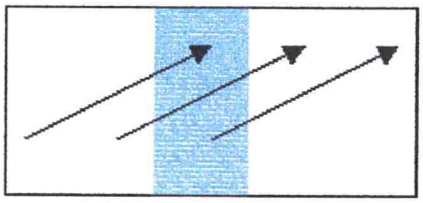

Figure 1.7. Schematic of charge particle equilibrium

The large distances required for CPE in air may be avoided by using a smaller thickness of an air-equivalent material having effective atomic number equal to that of air (Figure 1.8). The charge collected in the air volume originates in the air-equivalent wall of the chamber. The wall thickness required for electron equilibrium increases with radiation energy.

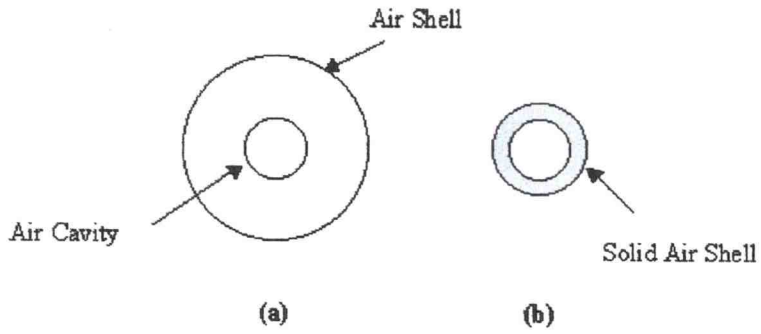

Figure 1.8. Diagram illustrating (a) an air shell with an air cavity (b) a solid air shell with an air cavity

For measurements in air of high-energy radiation beams, the walls of the chamber are not thick enough to provide equilibrium, so a buildup cap is used over the sensitive volume of the chamber. The buildup cap is usually made of acrylic (Plexiglas, Lucite) or Polystyrene.

A chamber with an air-equivalent wall, thick enough to provide electronic equilibrium and an accurately known volume is called a standard cavity chamber. Standard

cavity chambers are located at the National Institute of Standards and Technology (NIST) or at an Accredited Dosimetry Calibration Laboratory (ADCL). All ionization chambers with unknown volume are exposure-calibrated for a ^{60}Co beam against a standard cavity chamber. Exposure calibration factors (N_x) are obtained by placing the chambers in the same location as the standard chamber and giving them a known exposure. Because the wall thickness of these chambers is smaller then that required for electronic equilibrium, they are calibrated with a buildup cap over the sensitive volume of the chamber. This calibration procedure ensures that the calibrated clinical ion chambers are working properly.

1.6.1. Bragg-Gray theory

The total number of ion pairs produced is proportional to the energy absorbed by the medium. The conversion of ionization in the gas-filled cavity to absorbed dose in the medium is accomplished by applying Bragg-Gray theory. This theory is based on two assumptions. The first states that the air cavity must be small compared to the charged particle pathlength in air, and thus the charged particle fluence does not change inside the cavity. The second assumption asserts that all energy absorbed in the gas cavity is transferred by charged particles (Attix 1986).

Bragg-Gray cavity theory can be applied whether the field of charged particles enters from outside the vicinity of the cavity, as in case of an electron beam, or is generated in the medium through interactions by indirectly ionizing radiation, as in the case of a photon beam. In the latter case it is also assumed that no such interactions occur in the cavity gas. All charged particles in the Bragg-Gray cavity must originate elsewhere than in the cavity. Moreover, charged particles entering the cavity are assumed not to stop in it.

Suppose that a homogeneous medium (m) undergoing irradiation contains a small cavity filled with a gas (g). The "primary electrons" (original electrons or electrons generated by photons) give rise to ionization producing ion pairs. The average energy ($\bar{W}$) expended in the gas per ion pair formed (Attix 1986) can be determined according to:

$$\bar{W} = \frac{\text{Sum of all the kinetic energy spent in collision interactions by primary electrons}}{\text{Number of ion pairs produced by collision interactions by primary electrons}} \quad (1\text{-}2)$$

where $\bar{W}$ is a constant for each gas having units of electron-volt per ion pair, $\frac{eV}{i.p.}$. Table 1.2 shows the values of $\bar{W}$ for several gases (Attix 1986).

Table 1.2. Average energy ($\bar{W}$) expended per ion-pair formed in several gases

Gas	$\bar{W}$ (eV/i.p.)
H_2	36.5
N_2	34.8
O_2	30.8
CO_2	33.0

For gas mixtures $\bar{W}$ is given by

$$\left(\frac{1}{\bar{W}}\right)_{mixture} \cong \sum_i \left(\frac{P_i}{P}\frac{1}{\bar{W}_i}\right), \quad (1\text{-}3)$$

where P_i is the partial pressure of the i-th gas, and P is the total pressure of the mixture.

By dividing $\bar{W}$ by the charge of the electron in coulombs and converting energy from eV to Joules one obtains

$$\frac{\bar{W}}{e} \text{ in J/C} = \bar{W} \text{ in eV/i.p. x } \frac{1.602\text{x}10^{-19}\text{J/eV}}{1.602\text{x}10^{-19}\text{C/electron}}. \quad (1\text{-}4)$$

For air $\bar{W}$ equals 33.97 eV/i.p. and $\frac{\bar{W}}{e} = 33.97$ J/kg.

The absorbed dose in the air, D_{air}, in the cavity can be calculated by

$$D_{air} = J_{air}\frac{\bar{W}}{e}, \quad (1\text{-}5)$$

where J_{air} is the ionization charge of one sign produced per unit mass of the cavity gas in C/kg. The J_{air} can by written as:

$$J_{air} = \frac{M}{m} = \frac{M}{\rho_{air} V}, \tag{1-6}$$

where M is the charge measured by an electrometer, m is the mass, ρ is the density and V is the volume of gas.

If the cavity were replaced by an equal volume of medium, the absorbed dose in the medium would be

$$D_m = J_{air} \frac{\bar{W}}{e} \left[\left(\frac{\bar{S}}{\rho} \right)_{air}^{m} \right]_Q, \tag{1-7}$$

where $\left(\frac{\bar{S}}{\rho} \right)_{air}^{m}$ is a weighted mean ratio of the mass stopping power of the medium to that of the gas for the electrons crossing the cavity for a beam of quality Q (Khan 1984).

1.6.2. Spencer-Attix theory

Equation (1-7), as used in the determination of absorbed dose, is not quite correct because the average stopping power $\left(\frac{\bar{S}}{\rho} \right)$ does not take into account the fact that primary electrons may give rise to secondary fast moving electrons (δ-rays), and the energy they carry away is not excluded from the stopping power.

The effects of the δ-rays are accounted for in the Spencer-Attix formulation by using an arbitrary energy limit (Δ) below which energy transfers are considered dissipative (Attix 1986). The slow secondary electrons of energy less than Δ are assumed to dissipate their energy near the site of their release, while the fast ones, with energy above Δ are added to the "primary" electron spectrum. They carry enough energy to migrate within the cavity and deposit it elsewhere.

In Eq.(1-7), the mass stopping power $\left(\frac{\bar{S}}{\rho}\right)$ is replaced with the restricted stopping power $\left(\frac{\bar{L}}{\rho}\right)$ with Δ as the cutoff energy. The Spencer-Attix formulation of Bragg-Gray cavity theory uses the following relationship (Khan 1984):

$$D_m = J_{air} \frac{\bar{W}}{e} \left[\left(\frac{\bar{L}}{\rho} \right)_{air}^{m} \right]_Q \tag{1-8}$$

where $\left(\frac{\bar{L}}{\rho}\right)_{air}^{m}$ is the ratio of the average restricted mass stopping power of the medium to that of the gas for the electrons crossing the cavity for a beam of quality Q.

The value of Δ is somewhat arbitrarily taken to be the mean energy of electrons having ranges just large enough to cross the cavity (Spencer et al. 1955). Ion chamber diameters are between 0.2 and 0.8 cm, corresponding to electron ranges between 0.00024 and 0.00096 g/cm^2 in air. Consequently, for most cavity applications in ion chambers the value of Δ is between 10 and 20 keV, depending on their dimensions.

1.7. INTRODUCTION TO DOSIMETRY PROTOCOLS

In applications of ionizing radiation to problems in medicine, it is very important to measure with accuracy the amount of radiation delivered. The need for accurate dosimetry is greatest in radiation therapy for cancer because the typical doses delivered to tumors are very large, typically 10 times the dose which would kill a person receiving this dose to the entire body (Table 1.3). The doses also correspond to the steep portion of the dose-response curves (see Section 1.4). The effectiveness of the treatment depends on delivering the dose with an accuracy of $\pm$ 5% or better (Wambersie 1996).

Table 1.3. Curative doses of radiation for different cancer types

Type of cancer	Dose (Gy)
Skin cancer	40-45
Breast cancer	50-60
Head and neck	> 80

The dosimetry in different clinics has to be consistent and consequently national and international calibration protocols have been developed. Dosimetry protocols provide the radiological physicist with accurate methods for determining the dose-to-water from the high-energy photon and electron beams used in radiation therapy. Dose calibration means the determination of the radiation dose rate at a designated distance from a radiation source under specified conditions of measurement. In the US, the scientific society most involved in elaborating dosimetry protocols for the calibration of high-energy photon and electron beams is the American Association of Physicists in Medicine (AAPM). AAPM has published several protocols that incorporate the latest progress in radiation dosimetry at the time they were issued.

In 1971, the Scientific Committee on Radiation Dosimetry (SCRAD) of the AAPM published the first national protocol for photon and electron beams (Figure 1.9). This early protocol recommended that the response of an ionization chamber be characterized by an exposure calibration factor N_x traceable to a national standards laboratory. By application of the appropriate dose conversion factors (known as C_λ and C_E), phantom measurements for high-energy radiations these measurements were translated into absorbed dose. This early protocol did not take into account differences in the composition of the chamber wall or the dosimetry phantom. Also SCRAD did not consider the difference between the electron fluence in the cavity and the fluence in the medium which replaces the cavity.

In 1983 the AAPM Radiation Therapy Committee Task Group 21 published another protocol to address all the criticisms of the older protocol (Figure 1.9). The TG-21 protocol for the determination of the absorbed dose from high-energy photon and electron beams was based on a ^{60}Co exposure calibration factor (N_x) to determine the cavity

calibration factor (N_{gas}). The protocol is complex because it starts with a calibration for exposure, which is different from the clinical quantity of interest (absorbed dose), and the ionization chambers are calibrated in a ^{60}Co beam, while the radiotherapy is done with high-energy photon or electron beams. Also the dosimetry based on N_{gas} is dependent on external data which are not measured within the system. The complexity of this protocol could lead to reduced accuracy of clinical dosimetry, and result in mistakes.

Exposure plays a central role because it can be directly measured. In the last few years, many standard laboratories have developed new methods to directly measure the absorbed dose-to-water, replacing standards based on exposure with those based on absorbed-dose-to-water. The goal is to make clinical dosimetry much simpler and to improve its accuracy. In September 1999, the AAPM Radiation Therapy Committee Task Group 51 published a new external beam dosimetry protocol to replace the previous protocol (Figure 1.9). The TG-51 protocol relies on a ^{60}Co absorbed-dose-to-water calibration factor ($N_{D,w}^{^{60}Co}$) and an energy-dependent correction factor k_Q, which takes into account the variation of the absorbed dose-to-water calibration factor with the beam quality.

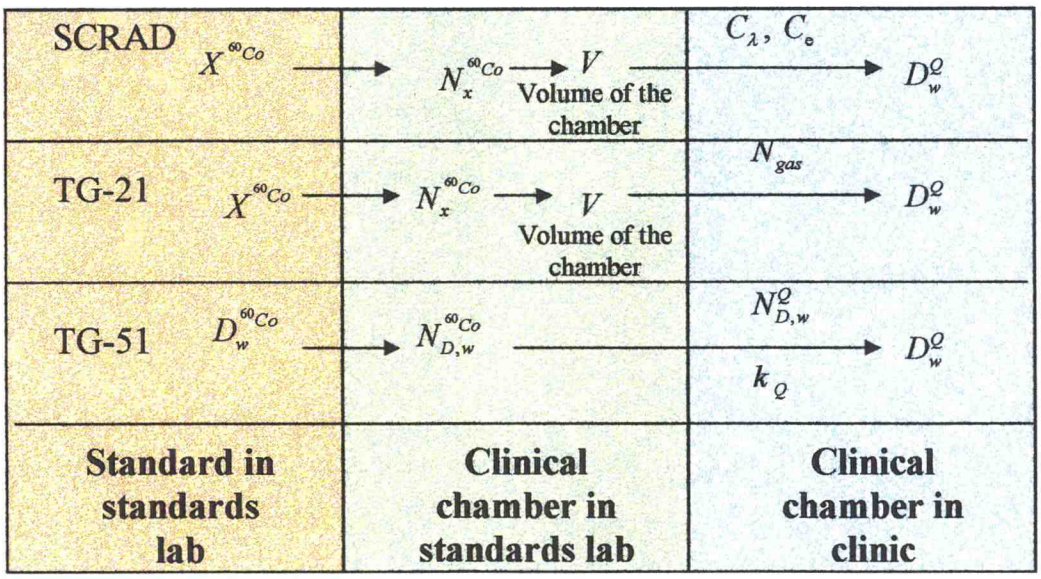

Figure 1.9. Protocol chains based on exposure and absorbed-dose calibrations

1.8. LITERATURE REVIEW AND THE OBJECTIVES OF THE STUDY

Medical clinics currently use linear accelerators of different make and models, and different types of ionization chambers. For clinical reference dosimetry the replacement of TG-21 with TG-51 protocol may result in changes in electron and photon beam output calibrations depending upon the accelerator, ionization chamber, the source of traceability (NIST or Canadian primary standards laboratories) and details of the protocol. The medical physicist should evaluate the implications of this transition at the clinic.

In 2000, Ding et al. compared the results of absorbed dose determined at reference conditions according to the AAPM TG-21 dose calibration protocol and the new AAPM TG-51 protocol. The photon beams of energies of 6 and 18 MV and the electron beams of energies from 6 to 20 MeV were created by Elekta SL20 and Siemens KD2 linear accelerators. Two cylindrical chambers (PR-06C and NE 2571) and two plane-parallel chambers (PTW Marcus, and Scanditronix NACP) with calibration factors traceable to the Canadian primary standards laboratory were used. The study showed that the dose changes are within 0.5% for photon energies of 6 and 18 MV, and 2%-3% for electron beams with energies of 6 to 20 MeV.

In the same year, Cho et al performed an experiment in which photon and electron beam outputs using both protocols were compared under identical conditions. Beam outputs were determined for 6 and 18 MV photon beams, and 9 and 16 MeV electron beams from a Clinac 2100 C following TG-21 and TG-51. The ionization chambers used in the study (NE 2571, PTW N23333, PTW N30001, PR-06C and Exradin A-12) had calibrations factors obtained from the ADCL at M.D Anderson Cancer Center-Houston, TX, based on standards traceable to NIST. The discrepancies between TG-21 and TG-51 were found to range between 0.2% and 1.1% for photon beams, and between 1.4% and 2.1% for electron beams.

One year later, in 2001, Huq et al. determined the absorbed dose-to-water in reference conditions with high-energy photon beams (6, 18 and 25 MV) generated by an Elekta MLCi and SL25 series linear accelerators. Two Farmer type ionization chambers (PTW 30001 and NE 2571) with calibrations traceable to NIST were used. Depending upon the choice of ionization chamber and beam quality, the discrepancy in absorbed dose-

to-water was found to range between 0.7% and 1.3%. The authors have also compared the two protocols for high-energy electron beams (6, 8, 10, 12, 15, and 18 MeV) generated by an Elekta MLCi linear accelerator. Six ionization chambers with calibration factors provided by the ADCL K & S Associates-Nashville, TN, based on standards traceable to NIST, two Farmer type (PTW 30001 and NE 2571) and four parallel chambers (PTW Marcus, and Scanditronix-Wellhofer NACP, PPC-05 and Roos PPC-40) were used. Depending upon the ionization chamber type used and beam energy the doses determined with TG-51 were higher than with TG-21 by about 1%-3%.

The present work was initiated in 2000 to address the questions regarding the impact of the implementation of TG-51 protocol at The Corvallis Cancer Center. The main objectives of the study were to determine the absorbed dose-to-water for photon and electron beams as recommended by TG-21 and TG-51 protocols and to compare the results. Also the study investigated the effects of the change from exposure to absorbed dose-to-water calibrated ionization chambers, and the effects of the change in beam quality specifier and restricted stopping powers on absorbed dose-to-water. A cylindrical Capintec PR-06G ionization chamber is used for dosimetric measurements. The chamber calibration factors were provided by the ADCL University of Wisconsin-Madison, WI, based on standards traceable to NIST. Photon beams of energies of 6 and 18 MV, and electron beams of 16 and 20 MeV were generated by a Clinac 2100 C linear accelerator, manufactured by Varian Medical Systems. Another objective of the study was to model the system in EGS4. The model was compared to photon and electron depth dose experimental data.

2. METHODS AND MATERIALS

2.1. ABSORBED DOSE CALCULATION ACCORDING TO AAPM TG-21 PROTOCOL

2.1.1. Basic equations and definitions

TG-21 protocol (AAPM 1983) recommends that the response of an ionization chamber be characterized by the cavity gas calibration factor (N_{gas}). Under those conditions the absorbed dose in air (D_{air}) can be written:

$$D_{air} = N_{gas} M \tag{2-1}$$

where M is an electrometer reading in Coulombs. The N_{gas} represents the calibration of the cavity air in terms of absorbed dose in the air per unit charge (Gy/C) and is unique to each ionization chamber, being related to the chamber volume. Substituting (1-5) and (1-6) into (2-1), and solving for N_{gas} yields

$$N_{gas} = \frac{1}{\rho_{air} V} \frac{\bar{W}}{e} \tag{2-2}$$

To determine N_{gas} one has to know the volume of the cavity. The chamber volume is not known to an acceptable accuracy for most ionization chambers. If this were a strictly mechanical measurement, the ion chamber could be made with sufficiently well known dimensions to specify the volume, but since the electric fields in these small chambers are not uniform, there are small regions from which the charge is not completely collected. In practice the volume can be determined if the chamber is ^{60}Co exposure-calibrated against a standard air chamber for determination of the exposure calibration factor N_x (Khan 1984).

Consider an ionization chamber that has been calibrated with a buildup cap for ^{60}Co exposure. First, one assumes that the buildup cap and chamber wall are composed of the same material. The exposure is then given by

$$X = M N_x, \tag{2-3}$$

where M is the charge measured with an electrometer and N_x is the exposure calibration factor (R/C) for ^{60}Co and is provided normalized to STP conditions (t=22 °C and p=1atm) by NIST or ADCL. This factor, which is a characteristic of the type of chamber, its volume and its buildup cap, is determined by exposing the chamber to a ^{60}Co beam of known exposure and comparing its response with a known exposure calibration factor for ^{60}Co. The absorbed dose in air can be determined by multiplying exposure with $\frac{\bar{W}}{e}$

$$D_{air} = X\frac{\bar{W}}{e}. \tag{2-4}$$

After substituting X given by (2-3) into (2-4), D_{air} can be written

$$D_{air} = MN_x\frac{\bar{W}}{e}. \tag{2-5}$$

If the chamber is replaced with a medium, the absorbed dose in the medium is given by (Khan 1984)

$$D_m = D_{air}\left[\left(\frac{\bar{\mu}_{en}}{\rho}\right)^m_{air}\right]_{^{60}Co}, \tag{2-6}$$

where $\left(\frac{\bar{\mu}_{en}}{\rho}\right)^m_{air}$ is the ratio of weighted mean mass energy absorption coefficient of the medium to that of air. Replacing D_{air} from (2-5) into (2-6) one obtains

$$D_m = MN_x\cdot\left[\frac{\bar{W}}{e}\left(\frac{\bar{\mu}_{en}}{\rho}\right)^m_{air}\right]_{^{60}Co} \tag{2-7}$$

Comparing (2-7) with (1-8), J_{air} can be written

$$J_{air} = MN_x\left[\left(\frac{\bar{\mu}_{en}}{\rho}\right)^m_{air}\left(\frac{\bar{L}}{\rho}\right)^{air}_m\right]_{^{60}Co}. \tag{2-8}$$

Considering a more realistic situation, in which the chamber has a wall of material (wl) and a buildup cap of material (b), a fraction α of air ionization is due to electrons generated in the wall, while the remaining $(1-\alpha)$ of air ionization is generated in the buildup cap. The J_{air} is then given by:

$$J_{air} = MN_x \cdot \left[\left(\alpha \left(\frac{\mu_{en}}{\rho} \right)_{air}^{wl} \left(\frac{\bar{L}}{\rho} \right)_{wl}^{air} + (1-\alpha) \left(\frac{\mu_{en}}{\rho} \right)_{air}^{b} \left(\frac{\bar{L}}{\rho} \right)_{b}^{air} \right) \right]_{^{60}Co} . \quad (2\text{-}9)$$

Substituting J_{air} in (1-6) and solving for volume of the cavity yields:

$$V = \frac{M}{\rho_{air} J_{air}} = \frac{1}{N_x \left[\left(\alpha \left(\frac{\mu_{en}}{\rho} \right)_{air}^{wl} \left(\frac{\bar{L}}{\rho} \right)_{wl}^{air} + (1-\alpha) \left(\frac{\mu_{en}}{\rho} \right)_{air}^{b} \left(\frac{\bar{L}}{\rho} \right)_{b}^{air} \right) \right]_{^{60}Co}} \quad (2\text{-}10)$$

Substituting V given by (2-10) into (2-2) yields (Khan 1984):

$$N_{gas} = N_x \frac{\bar{W}}{e} \left[\left(\alpha \left(\frac{\bar{\mu}_{en}}{\rho} \right)_{air}^{wl} \left(\frac{\bar{L}}{\rho} \right)_{wl}^{air} + (1-\alpha) \left(\frac{\bar{\mu}_{en}}{\rho} \right)_{air}^{b} \left(\frac{\bar{L}}{\rho} \right)_{b}^{air} \right) \right]_{^{60}Co} \quad (2\text{-}11)$$

The N_{gas} is further corrected for ion collection efficiency (A_{ion}), wall correction factor (A_{wall}), and quotient of absorbed dose by collision fraction of kerma (β):

- A_{ion} is the ionization collection efficiency at the time of calibration at NIST or ADCL, and applies to the in-air exposure calibration.
- A_{wall} takes into account the attenuation and scattering of the primary ^{60}Co beam in the wall and buildup cap of the ionization chamber. This correction relates the actual charge per unit mass of air in the chamber to that produced if there were neither attenuation nor scatter in wall and cap.
- β arises from the fact that the photon energy released at a point in the form of all charged particles (kerma) is transported distally and on the average imparted to the medium at some distal point. Thus, at any given point the absorbed dose is greater than the collision fraction of kerma.

So, the corrected N_{gas} can be determined from the formula:

$$N_{gas} = N_x \frac{\bar{W}}{e} \left[\left(\alpha \left(\frac{\bar{\mu}_{en}}{\rho} \right)_{air}^{wl} \left(\frac{\bar{L}}{\rho} \right)_{wl}^{air} + (1-\alpha) \left(\frac{\bar{\mu}_{en}}{\rho} \right)_{air}^{b} \left(\frac{\bar{L}}{\rho} \right)_{b}^{air} \right) A_{ion} A_{wall} \beta_w \right]_{^{60}Co} \quad (2\text{-}12)$$

The calculation of N_{gas} needs to be made only once, or anytime N_x is changed.

Knowing N_{gas}, D_{air} can determine according to (2-1). This relation is conceptually simple, but only applies for the ideal case. It assumes all the charge released is measured and it ignores the fact that the mass of air varies with temperature and pressure. Relation

(2-1) has to be further corrected for ion recombination loses (P_{ion}), and for standard conditions, t=22 °C and p=1 atm (P_{TP}).

$$D_{air} = MN_{gas}P_{ion}P_{TP} \tag{2-13}$$

- P_{ion} is a factor that corrects for ionization recombination losses. By making two sets of measurements, one with the normal bias potential applied to chamber, Q_1, and the other with the bias potential reduced to half, Q_2, P_{ion} is determined from Figure 4 of (AAPM 1983).
- P_{TP} makes the charge correspond to standard environment conditions for which the calibration factor applies. Since the exposure calibration factor is given for standard environmental conditions (22 °C, 1 atm), charge readings are corrected to standard conditions using (Khan 1984):

$$P_{TP} = \frac{T + 273^{\circ}C}{295^{\circ}C} x \frac{760mmHg}{P}. \tag{2-14}$$

Knowing D_{air} from (2-13) the absorbed dose in water can be calculated according to (1-8). Spencer-Attix theory assumes that the cavity has no wall or has a wall of the same material as the surrounding medium, so all the electrons crossing the cavity arise from the medium. Unfortunately, real ion chambers are not ideal cavities. There are several correction factors, which are needed before applying (1-8).

One of them is due to the heterogeneity of the chamber. Assume now a cavity with a wall of a different material than the medium in a photon beam of known quality (Q). Some of the electrons crossing the cavity will arise in the wall, others in the surrounding medium. If the electrons crossing the cavity arise entirely from photons interacting with the wall material (wl), Spencer-Attix theory yields:

$$D_{wl} = D_{air}\left[\left(\frac{\bar{L}}{\rho}\right)_{air}^{wl}\right]_Q, \tag{2-15}$$

where D_{wl} is the dose if the cavity air is replaced by wall material. If a medium replaces the wall material, the absorbed dose in the medium is given by (Khan 1984):

$$D_m = D_{wl}\left[\left(\frac{\bar{\mu}_{en}}{\rho}\right)_{wl}^{m}\right]_Q. \tag{2-16}$$

Combining (2-15) with (2-16) yields

$$D_m = D_{air}\left[\left(\frac{\bar{L}}{\rho}\right)_{air}^{wl}\left(\frac{\bar{\mu}_{en}}{\rho}\right)_{wl}^{m}\right]_Q . \tag{2-17}$$

If all the electrons crossing the cavity arise from the medium, the absorbed dose is

$$D_m = D_{air}\left[\left(\frac{\bar{L}}{\rho}\right)_{air}^{m}\right]_Q . \tag{2-18}$$

In practice a fraction α of the ionization arises from electrons released in the wall and a fraction $(1-\alpha)$ comes from electrons released in the medium. Thus, for the two-component model, by combining (2-17) with (2-18) and considering water (w) as medium yields

$$D_w = D_{air}\left[\left(\alpha\left(\frac{\bar{L}}{\rho}\right)_{air}^{wl}\left(\frac{\bar{\mu}_{en}}{\rho}\right)_{wl}^{w} + (1-\alpha)\left(\frac{\bar{L}}{\rho}\right)_{air}^{w}\right)\right]_Q . \tag{2-19}$$

Defining P_{wall} as follows

$$P_{wall} = \left[\frac{\alpha\left(\frac{\bar{L}}{\rho}\right)_{air}^{wl}\left(\frac{\bar{\mu}_{en}}{\rho}\right)_{wl}^{w} + (1-\alpha)\left(\frac{\bar{L}}{\rho}\right)_{air}^{w}}{\left(\frac{\bar{L}}{\rho}\right)_{air}^{wl}}\right]_Q , \tag{2-20}$$

the absorbed dose in water calculated according to (2-19) can be written as

$$D_w = D_{air}\left[\left(\frac{\bar{L}}{\rho}\right)_{air}^{w}\right]_Q P_{wall} . \tag{2-21}$$

The wall correction is unity when the chamber wall and dosimetry phantom are the same composition. Equation (2-21) allows the determination of the absorbed dose in a medium due to photons of quality Q. Assuming $P_{wall}=1$, the same formula applies also for electrons. If the walls and cavity are matched in atomic composition, the Bragg-Gray requirement for a small, non-perturbing cavity can be ignored, because according to Fano's theorem the charged-particle fluence at any point where CPE exists has a value that is independent of density variations within the volume of origin (Attix 1986). The validity of

Fano's theorem is undermined for megavolt photons because of the increasing importance of the "polarization effect", effect explained in Section 1.2 (Attix 1986).

The absorbed dose calculated according to (2-21) is further corrected for replacement:

$$D_w = D_{air}\left[\left(\frac{\bar{L}}{\rho}\right)_{air}^{w}\right]_Q P_{wall}P_{repl}\,. \qquad (2\text{-}22)$$

The replacement correction factor P_{repl} has two major components: gradient corrections and electron fluence corrections. Gradient corrections are required whenever the ionization chamber is at a location where the dose gradient has a nonzero slope (e.g. on the descending portion of the depth-dose curve). However most electron–beam dose calibrations are done with the chamber at d_{max} where gradient corrections are equal to 1. The depth d_{max} is the depth on the central axis at which an ionization chamber gives the maximum reading for electron and photon beams. Gradient corrections for cylindrical chambers depend on x-ray beam energy and the internal diameter of the chamber. Electron fluence corrections are required whenever the ionization chamber is at a location where charged-particle equilibrium has not been established (e.g. the dose-buildup region of high-energy x-ray beams and at all points in electron-beam dose distributions). Electron fluence corrections are not required for x-ray dose determinations made at or beyond d_{max} because a so-called "transient electron equilibrium" can be assumed to exist at these locations. The electron fluence correction for electron dose increases as the inner diameter of the chamber increases. It also increases as the mean energy of the electrons at the point of measurement decreases (Rogers 1996).

Substituting D_{air} from (2-13) into (2-22) yields the absorbed dose in water calculated by the TG-21 protocol (AAPM 1983):

$$D_{w,Q}^{TG-21} = MN_{gas}\left[\left(\frac{\bar{L}}{\rho}\right)_{air}^{w} P_{ion}P_{TP}P_{wall}P_{repl}\right]_Q . \qquad (2\text{-}23)$$

2.1.2. Beam quality

The doses calculated according to (2-23) are dependent upon the choice of the correct stopping-power ratios that are a function of the spectrum of electrons at the point of measurement, which in turn are a function of the energies of the incident x-rays or electrons. An ideal way to describe the quality of a radiation beam is to specify its spectral distribution. However, spectral distributions are difficult to measure so the protocol recommends that indices of beam quality be determined from in-phantom depth-ionization measurements. This recommendation will eliminate the errors that would occur from the fact that the spectra produced by accelerators operating at same energy may differ significantly, and so the stopping power ratios.

In megavoltage x-ray systems, beam quality is expressed in terms of the tissue phantom ratio (TPR), which is the ratio of the absorbed dose at a given depth in a phantom to the absorbed dose at the same point at a reference depth in phantom. If the reference depth is the depth of the absorbed dose maximum (d_{max}), the TPR is called the tissue maximum ratio (TMR). The beam quality is given by the ratio of ionization measurements made with a constant SAD and two different phantom thicknesses 10 and 20 cm, respectively

$$TPR_{10}^{20} = \frac{TPR_{20}}{TPR_{10}}. \tag{2-24}$$

The TPR_{10}^{20} is chosen as the beam quality for photon beams because it can be directly associated with the stopping power ratios.

The beam quality of electron beam is given in terms of the mean incident energy ($\bar{E}_0$) of electron beams at the phantom surface because, although an electron beam is almost monoenergetic before hitting the accelerator window, the random energy degradation which electrons suffer as they pass through the scattering foil, air and other materials results in the beam taking on a spectrum of energies at the phantom surface. Further degradation and spread of the beam energy takes place with depth into the phantom. The $\bar{E}_0$ is related to the depth at which ionization falls to 50% of its maximum (I_{50}):

$$\overline{E}_0 = CI_{50}. \tag{2-25}$$

where C=2.33 MeV cm^{-1} for water. The mean energy of the electron spectrum at depth z ($\overline{E}_z$) is given by

$$\overline{E}_z = \overline{E}_0\left(1-\frac{z}{R_p}\right). \tag{2-26}$$

The practical range (R_p) is the depth at the point where the tangent to the descending linear portion of the curve (at the point of inflexion) intersects the extrapolated background and can be determined using the depth ionization curve as shown in Figure 2.1 (Khan 1984). The $\overline{E}_0$ is chosen as the beam quality for electrons because it can be directly associated with stopping power ratios. In the TG-21 protocol the water to air stopping-power ratios needed for electron beam dosimetry are based on Monte Carlo calculations for monoenergetic electron beams.

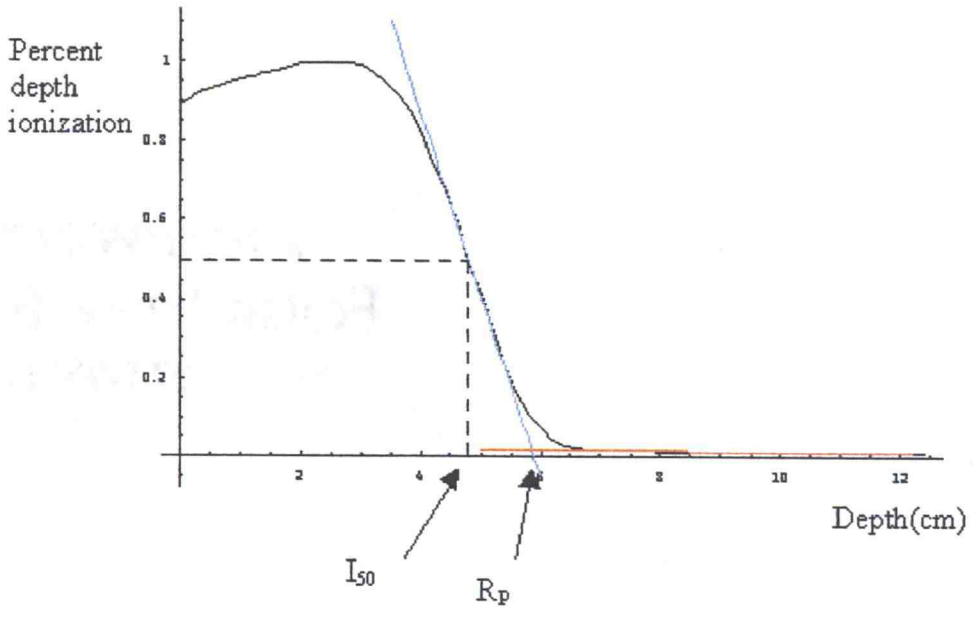

Figure 2.1. Depth dose curve illustrating the definition of I_{50} and R_p

2.1.3. Reference conditions of depth

Clinical reference dosimetry for photon and electron beams is performed in an open beam with the point of measurement (P) of the cylindrical ion chamber placed at the reference depth. The point of measurement of the cylindrical chamber is on the central axis. The effective point of measurement (P_{eff}) for a cylindrical chamber of radius (r) in a unidirectional beam is displaced by 0.75r from the point of measurement towards the source. This happens because electrons (from an electron beam or generated by photons) traversing the cylindrical chamber will enter the sensitive volume at different distances from the center of the chamber (Figure 2.2).

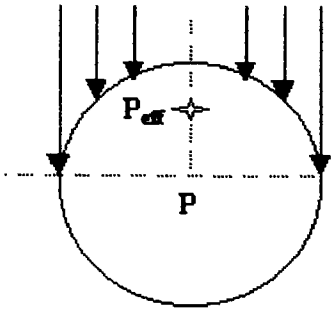

Figure 2.2. Diagram to illustrate the determination of the effective point of measurement for a cylindrical ionization chamber

For x-rays the calibration depth depends upon the inner diameter of the ionization chamber and the energy of the beam.

When an ionization chamber is used for dosimetry in electron beam radiotherapy, its response per unit absorbed dose in a water phantom varies with beam quality and measurement depth. The variation is determined mainly by the Spencer-Attix water to air stopping power ratio at the chosen point of measurement $\left(\frac{\bar{L}}{\rho}\right)_{air}^{w}$. For accurate reference dosimetry using a calibrated ion chamber one must specify the beam quality and the

reference depth in water in a manner which allows an accurate transfer of $\left(\frac{\bar{L}}{\rho}\right)_{air}^{w}$. In the TG-21 protocol the reference depth is chosen as the depth of the absorbed dose maximum, d_{max}.

2.2. ABSORBED DOSE CALCULATION ACCORDING TO AAPM TG-51 PROTOCOL

2.2.1. Basic equations and definitions

The formalism is based on the use of ionization chambers calibrated in terms of absorbed dose-to-water and quality factors at NIST or ADCL. The absorbed dose-to-water can be calculated using

$$D_w = MN_{D,w}^{Q}, \tag{2-27}$$

where M (C) is the electrometer reading and $N_{D,w}^{Q}$ (Gy/C) is the absorbed dose-to-water factor in an accelerator beam of quality Q. The direct determination of $N_{D,w}^{Q}$ in standard laboratories is problematic because of differences in accelerator beams. For this reason, the AAPM protocol starts from an absorbed-dose calibration factor in a ^{60}Co beam ($N_{D,w}^{^{60}Co}$) and introduces the quality conversion factor (k_Q) which takes into account the variation of absorbed dose calibration factor with the beam quality. Thus $N_{D,w}^{Q}$ is given by (Rogers 1996):

$$N_{D,w}^{Q} = k_Q N_{D,w}^{^{60}Co}. \tag{2-28}$$

Using (2-28) into (2-27) yields

$$D_w = Mk_Q N_{D,w}^{^{60}Co}, \tag{2-29}$$

where $N_{D,w}^{^{60}Co}$ is measured in the primary standards laboratory for each clinical chamber and M is measured in the clinic. Relation (2-29) has to be further corrected for recombination

loses, STP conditions, electrometer calibration and for polarity effects. The response of the chamber yielding the absorbed dose-to-water calculated according to the AAPM TG-51 protocol (AAPM 1999) is

$$D_{w,Q}^{TG-51} = Mk_Q N_{D,w}^{^{60}Co} P_{ion} P_{TP} P_{elec} P_{pol}, \tag{2-30}$$

where

- P_{ion} is the recombination correction factor. For pulsed beams the recombination factor can be determined by obtaining a reading at two different voltages and applying the equation (Weinhous et al. 1984):

$$P_{ion} = \frac{1 - V_H / V_L}{M^H / M^L - V_H / V_L} \tag{2-31}$$

  - M^H is the raw chamber reading with V_H the normal operating voltage for the detector
  - M^L is the raw chamber reading with chamber reading with bias $V_L = \frac{V_H}{2}$

- P_{TP} is the temperature-pressure correction factor as defined by (2-14).
- P_{elec} is the electrometer correction factor. If the electrometer is calibrated separately from the ion chamber, then the factor represents the electrometer calibration factor, which corrects the electrometer reading to true coulombs. The electrometer correction factor is 1, if the electrometer and ion chamber are calibrated as a unit.
- P_{pol} is the polarity correction factor, which takes into account polarity effects in the response of the ion chamber. To correct an ion chamber for polarity effects, measurements are taken with both polarities applied and the correction factor is deduced from the equation

$$P_{Pol} = \frac{M^+ - M^-}{2M^+} \tag{2-32}$$

  - M^+ is the reading when the positive charge is collected, and
  - M^- is the reading when the negative charge is collected.

2.2.2. Beam quality

For photon and electron beams the beam quality must be specified in order to determine the correct value of k_Q.

The photon beam quality TPR_{10}^{20} used in TG-21 is not the ideal beam quality specifier because stopping-power ratios $\left(\left(\frac{\bar{L}}{\rho}\right)_{air}^{w}\right)$ for the same value of TPR_{10}^{20} can vary significantly (Rogers 1996). In TG-51, the beam quality is specified by the percent depth dose at a reference distance of 10 cm in a water phantom due to photons only ($\%dd(10)_x$) (Kosunen et al. 1993). Percent depth dose (%dd) is the ratio, expressed as a percentage, of the absorbed dose at a given depth to the absorbed dose at a fixed reference depth, usually d_{max}. The %dd is dependent on four factors: energy, depth, field size, and SSD. The %dd increases as the energy, field size, and SSD increase. Higher energy radiations are more penetrating, so a greater percentage is available at a specific depth when compared to a lower energy. As field size increases, more scatter is added to the deposited beam, thus decreasing %dd. Percent depth dose decreases as the depth increases (inverse relationship), since dose is deposited in tissue with depth. The $\%dd(10)_x$ is the %dd(10) from which one has removed the effects of electron contamination from the measured value of the dose maximum by using a thin foil of lead (Li et al. 1994). The $\%dd(10)_x$ is a better specifier of beam quality than TPR_{10}^{20} in the sense that it almost uniquely determines the water to air stopping-power that applies at the reference depth in any photon beam (Rogers 1999).

If the energy is less than 10 MeV no lead is used to remove the electron contamination and $\%dd(10)_x$ will be equal to %dd(10). At higher energies the electrons from the accelerator head may significantly effect the dose at d_{max} and hence reduce the measured value of %dd(10). If the energy is greater than 10 MeV, a 1 mm Pb filter should be placed in the beam to reduce the effect of electrons from the accelerator (Rogers 1999). This lead foil should be placed at 50 ± 5 cm from the phantom surface, or if the accelerator construction does not permit a position near 50 cm, lead foil may be placed at 30 ± 1 cm. For this work the lead was placed at 29 cm and $\%dd(10)_x$ was calculated according to:

$$\%d(10)_x = [0.8116 + 0.00264\%dd(10)_{Pb}]\%dd(10)_{Pb} \quad \text{if } \%dd(10)_{Pb} > 71\%$$
$$\%dd(10)_x = \%dd(10)_{Pb} \quad \text{if } \%dd(10)_{Pb} < 71\% \tag{2-33}$$

Knowing $\%dd(10)_x$ from (2-33) and the chamber model, the value of k_Q is taken from Table I of (AAPM 1999).

For electron beams R_{50}, is chosen as a beam quality specifier for selecting stopping-power ratios and reference depths for electron dosimetry (Burns et al. 1996). The R_{50} represents the depth at which the absorbed dose falls to 50% of the maximum dose and can be determined according to

$$R_{50} = 1.029 I_{50} - 0.06 \text{ (cm)} \quad \text{for } 2 \le I_{50} \le 10 \text{ cm},$$
$$\text{or} \tag{2-34}$$
$$R_{50} = 1.059 I_{50} - 0.37 \text{ (cm)} \quad \text{for } I_{50} > 10 \text{ cm}$$

For electron beams, k_Q contains two components (Rogers et al. 1998):

$$k_Q = P_{gr}^Q k_{R_{50}} \tag{2-35}$$

where

- $k_{R_{50}}$ is a chamber-specific factor, defined as the product of two factors:

$$k_{R_{50}} = k'_{R_{50}} k_{ecal} \tag{2-36}$$

  - $k'_{R_{50}}$ is the electron quality conversion factor and is specified by the depth in water at which the absorbed dose falls to 50% of maximum dose (R_{50}). To determine R_{50} one must first measure a central-axis percent depth-dose curve in a water phantom.
  - k_{ecal} is a photon electron conversion factor associated with the conversion of the ^{60}Co absorbed dose calibration factor to an electron beam of quality (Q_e). The k_{ecal} is constant for a given chamber model.

- P_{gr}^Q is defined for cylindrical chambers to correct for gradient effects at reference depth. The value of this factor depends on the radius of the chamber

cavity and the ionization gradient at the point of measurement (AAPM 1999). For a cylindrical chamber of radius r_{cav} (cm), P_{gr}^{Q} is given by

$$P_{gr}^{Q} = \frac{M(d_{ref} + 0.5r_{cav})}{M(d_{ref})}. \tag{2-37}$$

The use of P_{gr}^{Q} is equivalent to making the measurement at the effective point of measurement.

2.2.3. Reference conditions of depth

Clinical reference dosimetry for photon and electron beams is performed in an open beam with the point of measurement of the cylindrical ion chamber placed at reference depth.

For photon beams the reference depth is 10 cm in a water phantom regardless of the photon energy. At this reference distance it has been proven that $\%dd(10)_x$ determines uniquely the water to air stopping-power ratio $\left(\frac{\bar{L}}{\rho}\right)_{air}^{w}$.

In TG-21, for electron beams, the recommended reference depth is d_{max}, which can be problematic. At incident energies above 10 MeV the value of d_{max} can vary by a large amount from machine to machine for beams of the same R_{50} because of the low energy electrons scattered into the phantom from the accelerator head (Burns et al. 1996). These scattered electrons increase the surface dose but do not significantly change R_{50}. It follows that the value of $\left(\frac{\bar{L}}{\rho}\right)_{air}^{w}$ at d_{max} will also vary between machines for beams of the same R_{50}. As a result, $\left(\frac{\bar{L}}{\rho}\right)_{air}^{w}$ must be expressed as a function of R_{50} and depth. It was found experimentally (Burns et al. 1996) that by adopting the electron reference depth

$$d_{ref} = 0.6R_{50} - 0.1 \text{ cm} \tag{2-38}$$

the $\left(\frac{\bar{L}}{\rho}\right)_{air}^{w}$ ratios become a function of R_{50} only. Using a single parameter to specify $\left(\frac{\bar{L}}{\rho}\right)_{air}^{w}$ rather than two parameters (R_{50} and depth) has the potential to greatly simplify electron beam dosimetry protocols.

2.3. COMPARISON BETWEEN DOSE AND EXPOSURE STANDARDS

The discrepancies between the two protocols due to the changes of calibration factors and beam quality specifiers, can be explained by comparing the absorbed dose-to-water determined according to TG-51 protocol ($D_{w,Q}^{TG-51}$) and the absorbed dose-to-water determined using TG-51 equations, but with $N_{D,w}^{^{60}Co}$ and k_Q based on TG-21 data $\left(\left(D_{w,Q}^{TG-51}\right)_{\substack{TG-21\\data}}\right)$.

The relationship between $N_{D,w}^{^{60}Co}$ and N_{gas} can be derived by comparing the absorbed dose-to-water determined for a ^{60}Co beam using TG-51 and TG-21 protocols. $D_{w,^{60}Co}^{TG-51}$ and $D_{w,^{60}Co}^{TG-21}$ calculated using (2-30) and (2-23) for ^{60}Co can be written

$$D_{w,^{60}Co}^{TG-51} = M_{^{60}Co} N_{D,w}^{^{60}Co} \left[P_{ion} P_{TP}\right]_{^{60}Co}, \quad (k_Q = 1,\ P_{elec} = 1) \tag{2-39}$$

and

$$D_{w,^{60}Co}^{TG-21} = M_{^{60}Co} N_{gas} \left[\left(\frac{\bar{L}}{\rho}\right)_{air}^{water} P_{ion} P_{TP} P_{wall} P_{repl}\right]_{^{60}Co}. \tag{2-40}$$

Equating (2-37) and (2-38) and solving for $N_{D,w}^{^{60}Co}$ yields

$$\left(N_{D,w}^{^{60}Co}\right)_{\substack{TG-21\\data}} = N_{gas} \left[\left(\frac{\bar{L}}{\rho}\right)_{air}^{water} P_{wall} P_{repl}\right]_{^{60}Co}. \tag{2-41}$$

Similarly, the absorbed dose-to-water factor in an accelerator beam of quality Q can be calculated from

$$\left(N_{D,w}^{Q}\right)_{\substack{TG-21\\data}} = N_{gas}\left[\left(\frac{\bar{L}}{\rho}\right)_{air}^{water} P_{wall}P_{repl}\right]_{Q} . \qquad (2\text{-}42)$$

The beam quality conversion factor k_Q defined in (2-28) can be written (Rogers 1996) by using (2-40) and (2-39) as:

$$\left(k_Q\right)_{\substack{TG-21\\data}} = \frac{\left(N_{D,w}^{Q}\right)_{\substack{TG-21\\data}}}{\left(N_{D,w}^{^{60}Co}\right)_{\substack{TG-21\\data}}} = \frac{\left[\left(\frac{\bar{L}}{\rho}\right)_{air}^{water} P_{wall}P_{repl}\right]_{Q}}{\left[\left(\frac{\bar{L}}{\rho}\right)_{air}^{water} P_{wall}P_{repl}\right]_{^{60}Co}} . \qquad (2\text{-}43)$$

The absorbed dose-to-water determined using the TG-51 equations, and $N_{D,w}^{^{60}Co}$ and k_Q factors from TG-21 data can be written

$$\left(D_{w,Q}^{TG-51}\right)_{\substack{TG-21\\data}} = M\left(k_Q\right)_{\substack{TG-21\\data}}\left(N_{D,w}^{^{60}Co}\right)_{\substack{TG-21\\data}}\left[P_{ion}P_{TP}\right]_{Q} \qquad (2\text{-}44)$$

The ratio of $D_{w,Q}^{TG-51}$ and $\left(D_{w,Q}^{TG-51}\right)_{\substack{TG-21\\data}}$ calculated according to (2-30) and (2-42) respectively is equal to

$$\frac{D_{w,Q}^{TG-51}}{\left(D_{w,Q}^{TG-51}\right)_{\substack{TG-21\\data}}} = \frac{k_Q}{\left(k_Q\right)_{\substack{TG-21\\data}}}\frac{N_{D,w}^{^{60}Co}}{\left(N_{D,w}^{^{60}Co}\right)_{\substack{TG-21\\data}}} . \qquad (2\text{-}45)$$

2.4. MATERIALS

Photon beams of energies 6 and 18 MV and electron beams of 16 and 20 MeV were generated by using a Varian Clinac 2100 C linear accelerator. The beams were normal incident on the phatom surface. The ionization chambers used in this study were cylindrical Capintec PR-05 and PR-06G (SN#CII.668747) of volume 0.14 cm^3 and 0.6 cm^3

respectively. A description of the PR-06G and PR-05 ionization chambers can be found in Appendices C and D. The calibration factors, as provided by an ADCL, are $N_{D,w}^{^{60}Co} = 5.008x10^7 Gy/C$ and $N_x = 5.173x10^9 R/C$ as shown in Appendices A and B. Knowing N_x, one calculates N_{gas} according to (2-12).

The measurements were performed in a water phantom. Water was the material used for the dosimetry phantom because it approximates the radiation absorption and scattering properties of muscle and other soft tissues. The water phantom poses some practical problems when used in conjunction with the ionization chamber, which is effected by water. Thus, before immersion into the water phantom the detector was placed into a thin plastic sleeve, made of polymethylmethacrylate (PMMA). Before performing the measurements, the phantom and ionization chamber were let for several hours, so their temperature became equal to the room temperature. For a given energy, the TG-21 and TG-51 measurements were performed at the same temperature. An appropriate correction was applied to determine dose at standard environmental conditions (1 atm and 22°C). Each measurement was performed over a period of time equal to 200 monitor units (MU). The MU is an arbitrary unit of measure for time.

2.4.1. Photon beams

The beam quality of the photon beams for the TG-21 protocol was determined as the ratio of the tissue to phantom ratios at 20 and 10 cm depth in water, TPR_{10}^{20}. A field of size 10x10 cm^2 and a SAD=100 cm were used. Knowing the ionization ratio it was possible to determine the nominal accelerating potential, P_{repl}, α, $\left(\frac{\bar{L}}{\rho}\right)_{air}^{water}$, $\left(\frac{\bar{\mu}}{\rho}\right)_{air}^{water}$ and P_{wall} from Fig.3, Fig.5, Fig.7, Fig.2, Table IX of (AAPM 1983) and equation (2-20). The ionization recombination correction factors P_{ion} were determined using Fig.4 of (AAPM 1983), where Q_1/Q_2 is the ratio of electric charge measurements with 300 V and 150 V, respectively, applied to the chamber.

The beam quality of photon beams for the TG-51 protocol was determined for SSD=100 cm and a 10x10 cm^2 field size. The chamber used for the beam quality determination was a Capintec PR-05 ionization chamber (r_{cav}=2 mm). The point of measurement of the chamber was positioned at (d_{ref}+0.6r_{cav}), d_{ref}=10 cm, to ensure that the effective point of measurement is at d_{ref}. For the 6MV photon beam, %dd(10) was taken to be equal to $\%dd(10)_x$. For the 18 MV photon beam, $\%dd(10)_x$ was obtained following the procedure described in Section 2.2.2, using a 1 mm lead foil placed at 29 cm. Knowing $\%dd(10)_x$ the quality conversion k_Q can be determined from Table I of (AAPM 1999). The recombination correction factors P_{ion} were determined according to (2-31), with V_H=300 V and V_L=150 V. The polarity correction factors were determined according to (2-32) with +300 V and –300 V potentials applied to the chamber.

The dose determinations according to TG-21 and TG-51 are based in both cases on measurements taken with a 10x10 cm^2 field size at SAD=100 cm, using a Capintec PR-06G ionization chamber. The calibration depth, according to TG-21, depends upon the energy of the beam. For the 6 MV beam, the calibration depth was 5 cm, and for the 18 MV, the depth was 7 cm. These values were taken from Table XI of (AAPM 1983). According to the TG-51 protocol the calibration depth was 10 cm for all photon energies. Because the depths of calibration recommended in the TG-21 protocol differ from those recommended in the TG-51 protocol, d_{max} is chosen to compare the absorbed dose-to-water from to the two protocols.

2.4.2. Electron beams

All electron beam measurements were made with a 15x15 cm^2 field size at SSD=100 cm, using a Capintec PR-06G ionization chamber. For the beam quality determination, measurements were performed at various depths. The percent ionization was plotted against depth for various electron beam energies. Based on these graphs R_{50}, R_P and d_{max} were determined.

According to TG-21, the mean incident energy $\bar{E}_0$ and mean electron energy at depth of measurement $\bar{E}_z$ can be calculated from (2-25) and (2-26) respectively. Knowing $\bar{E}_0$ and $\bar{E}_z$, $\left(\frac{\bar{L}}{\rho}\right)_{air}^{water}$ and P_{repl} were determined from Table V and VIII of (AAPM 1983). The ionization recombination correction factors P_{ion} are determined from Fig.4 of (AAPM 1983) where Q_1/Q_2 is the ratio of electric charge measurements with 300 V and 150 V applied to the chamber.

According to TG-51, knowing R_{50} determines $d_{ref}=0.6R_{50}-0.1$. The point of measurement of the ionization chamber was placed at $(d_{ref}+0.5r_{cav})$. From Fig.5 of (AAPM 1999) $k'_{R_{50}}$ can be found. The recombination correction factors P_{ion} were determined according to (2-31), with V_H=300V and V_L=150V. Polarity correction factors were determined according to (2-32) with +300V and –300V potentials applied to the chamber.

The calibration depths based on TG-21 for 16 and 20 MeV were 3.3 and 2.0 cm respectively, while those based on TG-51 were 3.83 and 4.814 cm respectively. Using the corrected readings the absorbed doses were determined. Because the depths of calibration recommended in the TG-21 protocol differ from those recommended in the TG-51 protocol, d_{max} is chosen to compare the absorbed dose-to-water determined by the two protocols.

2.5. ABSORBED DOSE DETERMINATION USING EGS4

Monte Carlo transport techniques are recognized as the desired method of computing patient dose. They improve the accuracy of clinical dosimetry by providing more realistic data. The Monte Carlo method for radiation transport problems simulates the tracks of individual particles by sampling appropriate quantities from the probability distributions governing the individual physical processes using machine-generated pseudo-random numbers. Average values of macroscopic quantities such as particle fluence, energy spectrum and absorbed dose distribution can be evaluated by simulating a large number of particle histories.

A Monte Carlo treatment planning system needs detailed information about the beams incident on the patient. The most practical way to obtain detailed information about the incident radiation beam is a Monte Carlo simulation of the head of the medical accelerator. A full Monte Carlo simulation of the medical geometry is a very difficult task. Information on material composition, dimensions, distances and overall design of internal filters and collimators is vital to producing an accurate model of the photon and electron spectrum. Unfortunately this information is proprietary and was unavailable. In this study, instead of modeling the head of the accelerator, monoenergetic electron beams and realistic photon spectra obtained at the National Research Council of Canada (NRC) by full Monte Carlo simulations of a Varian Clinac 2100 C linear accelerator using the BEAM code are used as radiation sources. BEAM is a general purpose Monte Carlo simulation code that allows the simulation of radiotherapy treatment units and produces data on realistic clinical beams. It has been extensively benchmarked against measured dose distributions for a variety of accelerators and good agreement has been obtained in central-axis percentage depth-dose (Rogers et al.1995).

"Electron Gamma Shower" (EGS4) is the Monte Carlo code commonly used in medical physics (EGS4 1985). EGS4 is compared and evaluated against photon and electron depth dose experimental data. The modeling of the system is performed according to TG-21 and TG-51. The 6 MV and 18 MV photon spectra (Appendix E), obtained at NRC with the BEAM code, are used as photon spectra in EGS4. Two monoenergetic electron beams, 16 and 20 MeV are used as electron sources. Circular fields of radius 5.6 and 7 cm are used to approximate square fields of 10x10 for photons and 15x15 cm^2 for electrons, respectively.

3. RESULTS AND DISCUSSION

The doses-to-water per monitor unit for 6 and 18 MV energy photon beams calculated according to TG-21 and TG-51, respectively are shown in Table 3.1.

Table 3.1. Absorbed dose-to-water determined according to TG-21 and TG-51 protocols, for 6 and 18 MV energy photon beams

Energy (MV)	$D^{TG-21}(Gy/MU)$	$D^{TG-51}(Gy/MU)$	$\frac{D^{TG-51}(Gy/MU)}{D^{TG-21}(Gy/MU)}$
6	0.990	1.004	1.014
18	0.994	1.011	1.017

Table 3.1 shows a discrepancy of about 1.4% and 1.7% between the absorbed dose-to-water determined according to the TG-21 and TG-51 protocols for 6 MV and 18 MV energy photon beams, respectively. The results of the measurements and calculations are shown in detail in Appendix F. The uncertainties affecting D^{TG-21} and D^{TG-51} have been estimated to be approximately 1% and 0.5% for both photon beam energies, respectively.

Table 3.2 shows the doses to water per monitor unit for 16 and 20 MeV energy electron beams calculated according to TG-21 and TG-51, respectively.

Table 3.2. Absorbed dose-to-water determined according to TG-21 and TG-51 protocols, for 16 and 20 MeV energy electron beams

Energy (MeV)	$D^{TG-21}(Gy/MU)$	$D^{TG-51}(Gy/MU)$	$\frac{D^{TG-51}(Gy/MU)}{D^{TG-21}(Gy/MU)}$
16	0.998	1.016	1.018
20	0.994	1.018	1.024

Absorbed doses-to-water per monitor unit determined according to TG-21 and TG-51 for 16 MeV energy electron beams agree within 1.8%, while the data for the 20 MeV beam agree to within 2.4%. The results of the measurements and calculations are shown in detail in Appendix F. The uncertainties affecting D^{TG-21} and D^{TG-51} have been estimated to be approximately 0.5% for both electron beam energies. For electron beams, the measured percent depth ionization is plotted against depth for 16 and 20 MeV energy electron beams. The measured data is presented in Figure 3.1, 3.2 and Appendix G.

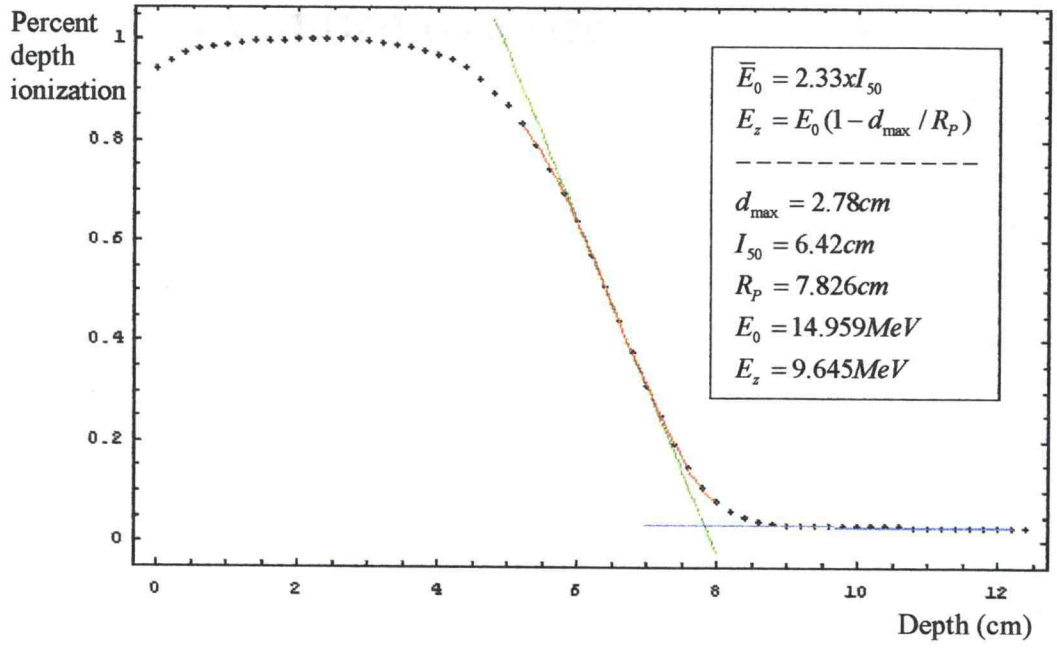

Figure 3.1. Measured percent depth ionization curve for a 16 MeV energy electron beam. (SSD=100 cm; field size=15x15 cm^2)

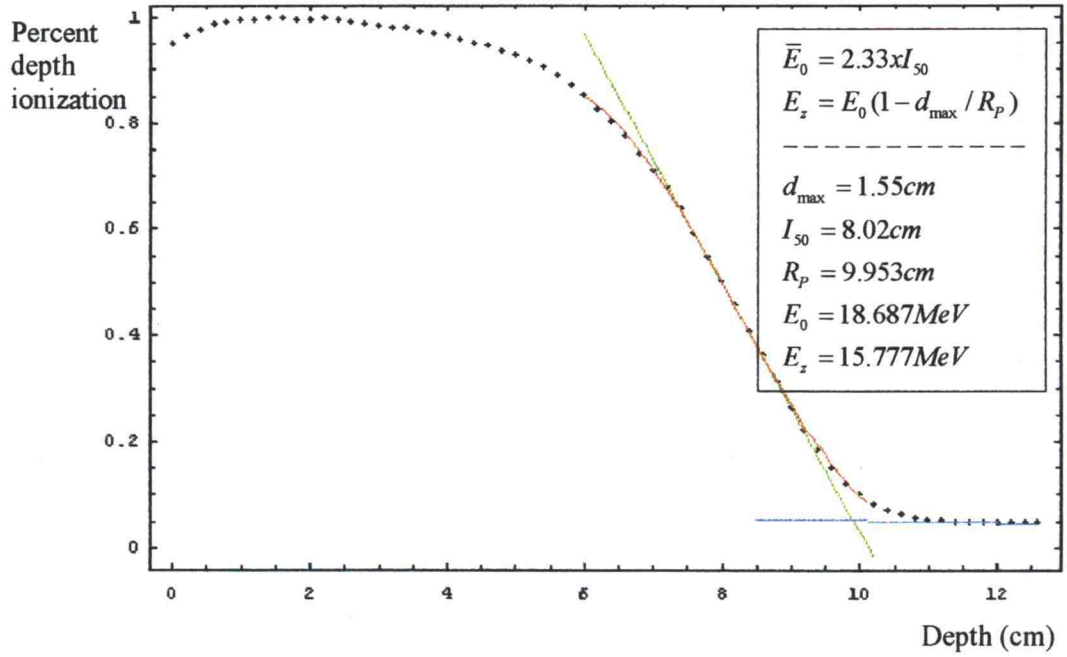

Figure 3.2. Measured percent depth ionization curve for a 20 MeV energy electron beam. (SSD=100 cm; field size=15x15 cm^2)

Table 3.3 shows that the discrepancies between the TG-21 and TG-51 protocols found in the present work are close to those reported by other authors that have used different types of ionization chambers with calibration factors traceable to NIST or Canadian primary standards laboratory and/or different linear accelerators.

Table 3.3. Discrepancies between the absorbed dose-to-water determined according to TG-21 and TG-51 protocols by various authors

Type of beam	**Discrepancies between TG-51 and TG-21 (%)**			
Photons	(Ding 2000)	(Huq et al. 2001)	(Cho et al. 2000)	Present work
6 and 18 MV	0.5	Up to 1	Up to 1	1-2
Electrons	(Ding 2000)	(Huq et al. 2001)	(Cho et al. 2000)	Present work
16 and 20 MeV	2-3	1-3	Up to 2	1-3

The discrepancies between TG-21 and TG-51 due to the changes from exposure to absorbed dose-to-water calibration factor and beam quality specifiers can be highlighted by determining the absorbed dose-to-water using TG-51 equations but calculating k_Q and $N_{D,w}^{^{60}Co}$ using TG-21 data. The data are summarized in Table 3.4 and Table 3.5 for photon and electron beams, respectively. The $\left(N_{D,w}^{^{60}Co}\right)_{\substack{TG-21\\data}}$, $\left(k_Q\right)_{\substack{TG-21\\data}}$ and $\left(D_{w,Q}^{TG-51}\right)_{\substack{TG-21\\data}}$ are calculated with (2-41), (2-43) and (2-44).

Table 3.4. Comparison between absorbed dose-to-water data determined according to the TG-51 protocol and data calculated using TG-51 equations but TG-21 data for 6 and 18 MV photon beams

Quantities to compare	**6 MV**	**18 MV**
N_{gas} (cGy/C)	$4.399\text{x}10^9$	$4.399\text{x}10^9$
$N_{D,w}^{^{60}Co}(cGy/C)$	$5.008\text{x}10^9$	$5.008\text{x}10^9$
$\dfrac{N_{D,w}^{^{60}Co}}{N_{gas}}$	1.1384	1.1384
$\dfrac{\left(N_{D,w}^{^{60}Co}\right)_{\substack{TG-21\\data}}}{N_{gas}}$	1.1140	1.1140
$\dfrac{N_{D,w}^{^{60}Co}}{\left(N_{D,w}^{^{60}Co}\right)_{\substack{TG-21\\data}}}$	1.022	1.022
k_Q	0.994	0.970
$\left(k_Q\right)_{\substack{TG-21\\data}}$	0.999	0.978
$\dfrac{k_Q}{\left(k_Q\right)_{\substack{TG-21\\data}}}$	0.995	0.992
$\dfrac{D_{w,Q}^{TG-51}}{\left(D_{w,Q}^{TG-51}\right)_{\substack{TG-21\\data}}}$	1.017	1.014

Table 3.5. Comparison between absorbed dose-to-water determined according to the TG-51 protocol and data calculated using TG-51 equations but TG-21 data for 16 and 20 MeV electron beams

Quantities to compare	16 MeV	20 MeV
N_{gas} (cGy/C)	4.399x10^9	4.399x10^9
$N_{D,w}^{^{60}Co}(cGy/C)$	5.008x10^9	5.008x10^9
$\frac{N_{D,w}^{^{60}Co}}{N_{gas}}$	1.1384	1.1384
$\frac{\left(N_{D,w}^{^{60}Co}\right)_{\substack{TG-21 \\ data}}}{N_{gas}}$	1.1140	1.1140
$\frac{N_{D,w}^{^{60}Co}}{\left(N_{D,w}^{^{60}Co}\right)_{\substack{TG-21 \\ data}}}$	1.022	1.022
k_Q	0.899	0.887
$\left(k_Q\right)_{\substack{TG-21 \\ data}}$	0.896	0.880
$\frac{k_Q}{\left(k_Q\right)_{\substack{TG-21 \\ data}}}$	1.003	1.008
$\frac{D_{w,Q}^{TG-51}}{\left(D_{w,Q}^{TG-51}\right)_{\substack{TG-21 \\ data}}}$	1.025	1.030

The change from exposure to absorbed dose-to-water calibrated ionization chambers has the strongest impact on the differences between TG-21 and TG-51 absorbed dose-to-water, while the change in beam quality specifier and stopping power ratios have only a very small effect on these differences.

The difference between the measured $\frac{N_{D,w}^{^{60}Co}}{N_{gas}}$ and the calculated $\frac{\left(N_{D,w}^{^{60}Co}\right)_{\substack{TG-21 \\ data}}}{N_{gas}}$ is 2.2%, the measured value being higher than the calculated one.

Table 3.4 shows that the differences between TG-51 values of k_Q and the ones calculated using TG-21 data are 0.4% and 0.8% for 6 and 18 MV energy photon beams, respectively, the TG-51 values being smaller than the calculated ones. The discrepancy originates from differences in the water-to-air stopping power ratios. For photon beams, the TG-21 protocol uses stopping powers from ICRU Report 35 (ICRU 1984), whereas the TG-51 protocol uses ICRU Report 37 (ICRU 1984). The ICRU Report 37 reviews topics such as density effect, restricted stopping power, radiative stopping power, ranges and radiation yields.

For photon beams the effects due to the calibration and beam quality conversion factors cancel. Thus the discrepancies between the absorbed dose-to-water determined according to the TG-51 protocol and that calculated using equations from TG-51 but determining k_Q and $N_{D,w}^{^{60}Co}$ using TG-21 data, are only 1.7% and 1.4% for 6 and 18 MV energy photon beams, respectively as shown in Table 3.4. Comparing these discrepancies with the ones from Table 3.1, one can see that they are very close. This implies that the sources of the observed discrepancies between the two types of protocols come mostly from calibration factors and beam quality specifications.

Table 3.5 shows that the differences between TG-51 values of k_Q and the ones calculated using TG-21 data are 0.3% and 0.8% for 16 and 20 MeV electron beam energies, respectively, the TG-51 values being larger than the calculated ones. This discrepancy can be explained by the differences between the stopping-power ratios. Although both protocols use stopping-power values from ICRU Report 35, the TG-21 protocol uses stopping-power ratios calculated for monoenergetic electron beams, while the TG-51 protocol, by changing to a new reference depth for electron beams defined by $d_{ref}=0.5R_{50}-0.1$ cm, uses the stopping-power ratios calculated for realistic electron beams. The d_{ref} is equal to the d_{max} for low-energy electron beams but is deeper than d_{max} for high-energy electron beams.

As shown in Table 3.5, for electron beams the effects originating from calibration and beam quality conversion factors amplify, and the discrepancies between the absorbed dose-to-water determined according to the TG-51 protocol and that determined using the TG-51 equations but calculating k_Q and $N_{D,w}^{^{60}Co}$ with TG-21 data, are 2.5% and 3.0% for 16 and 20 MeV energy electron beams, respectively. As shown in Table 3.2 the differences in absorbed doses determined according to the TG-51 and TG-21 protocols for 16 and 20 MeV energy electron beams were 1.8% and 2.4%, respectively. As in the case of photons, these values were very close with those calculated. This implies that the sources of the observed discrepancies between the two types of protocols are the calibration factors and beam quality specifications.

Photon spectra of 6 and 18 MV energies obtained at NRC by full Monte Carlo simulations of Varian Clinac 2100 C using the code BEAM (Rogers et al. 1995) were used as input to the EGS4 code to predict percent depth doses. The results are shown in Figure 3.3 and Figure 3.4. The uncertainties effecting the EGS4 calculations are approximately 0.2% for both photon beam energies.

The absorbed dose-to-water for photons determined according to TG-21 and TG-51 were compared with that calculated by EGS4. For a 6MV energy photon beam, the EGS4 and the TG-21 percent depth doses differ by 1.3%, while EGS4 and TG-51 percent depth doses differ by 4.4%. For an 18 MV energy photon beam the EGS4 and TG-21 percent depth doses differ by 1.2%, while EGS4 and TG-51 percent depth doses differ by 3.1%. These data are summarized in Table 3.6.

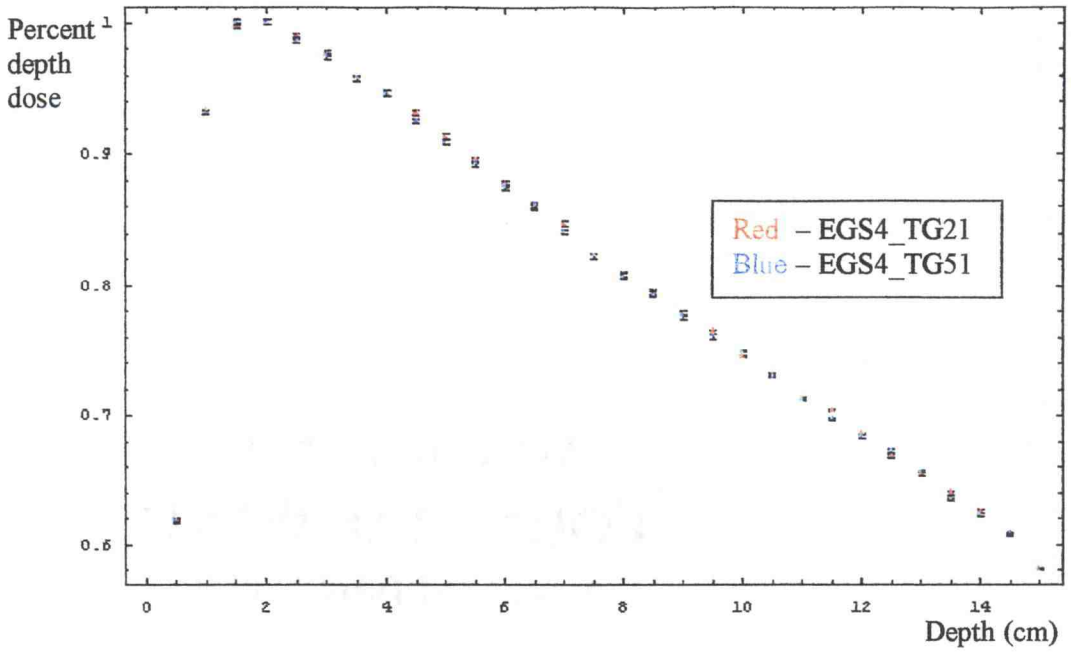

Figure 3.3. Percent depth dose curve obtained with EGS4 for a 6 MV energy photon beam

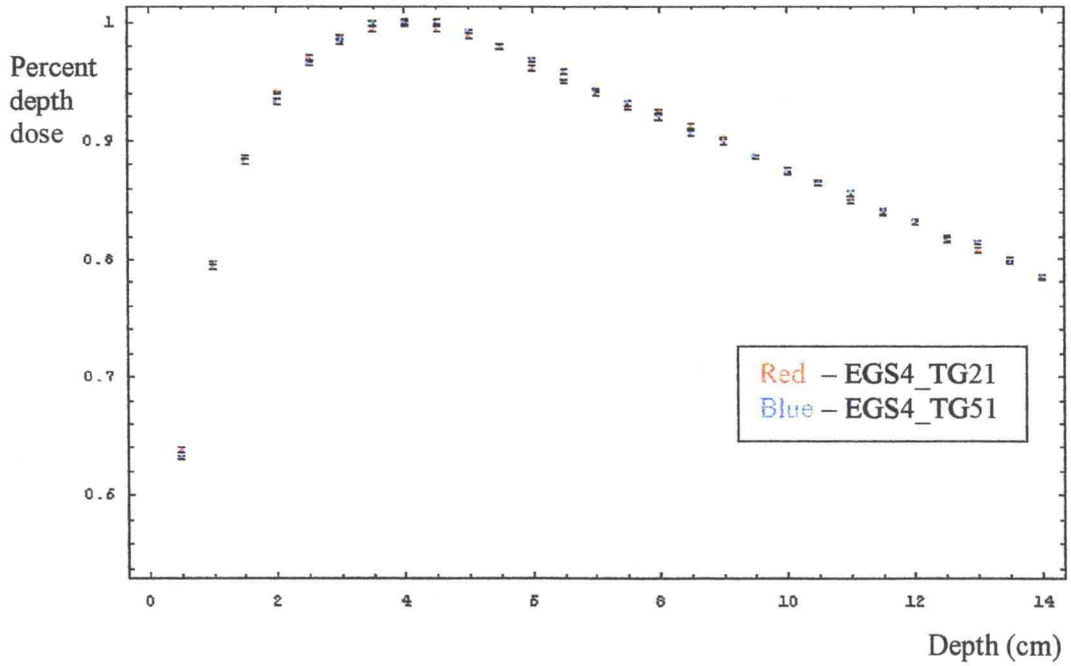

Figure 3.4. Percent depth dose curve obtained with EGS4 for a 18 MV energy photon beam

Table 3.6. Results of dose comparison between the TG-21, TG-51 protocols and EGS4

6 MV		18 MV	
$\left(\frac{D^{TG-21}(5cm)}{D^{TG-21}(d_{max}=1.5cm)}\right)_{exp}$	0.921	$\left(\frac{D^{TG-21}(7cm)}{D^{TG-21}(d_{max}=4cm)}\right)_{exp}$	0.961
$\left(\frac{D^{TG-21}(5cm)}{D^{TG-21}(d_{max}=1.5cm)}\right)_{EGS4}$	0.909	$\left(\frac{D^{TG-21}(7cm)}{D^{TG-21}(d_{max}=4cm)}\right)_{EGS}$	0.949
$\frac{\left(\frac{D^{TG-21}(5cm)}{D^{TG-21}(d_{max}=1.5cm)}\right)_{exp}}{\left(\frac{D^{TG-21}(5cm)}{D^{TG-21}(d_{max}=1.5cm)}\right)_{EGS4}}$	1.013	$\frac{\left(\frac{D^{TG-21}(7cm)}{D^{TG-21}(d_{max}=4cm)}\right)_{exp}}{\left(\frac{D^{TG-21}(7cm)}{D^{TG-21}(d_{max}=4cm)}\right)_{EGS}}$	1.013
$\left(\frac{D^{TG-51}(10cm)}{D^{TG-51}(d_{max}=1.5cm)}\right)_{exp}$	0.773	$\left(\frac{D^{TG-51}(10cm)}{D^{TG-51}(d_{max}=4cm)}\right)_{exp}$	0.908
$\left(\frac{D^{TG-51}(10cm)}{D^{TG-51}(d_{max}=1.5cm)}\right)_{EGS4}$	0.739	$\left(\frac{D^{TG-51}(10cm)}{D^{TG-51}(d_{max}=4cm)}\right)_{EGS4}$	0.880
$\frac{\left(\frac{D^{TG-51}(10cm)}{D^{TG-51}(d_{max}=1.5cm)}\right)_{exp}}{\left(\frac{D^{TG-51}(10cm)}{D^{TG-51}(d_{max}=1.5cm)}\right)_{EGS4}}$	1.046	$\frac{\left(\frac{D^{TG-51}(10cm)}{D^{TG-51}(d_{max}=4cm)}\right)_{exp}}{\left(\frac{D^{TG-51}(10cm)}{D^{TG-51}(d_{max}=4cm)}\right)_{EGS4}}$	1.032

The EGS4 results are closer to the TG-21 results than to the TG-51 results. This can be explained by the fact that the EGS4 version used in this work used the stopping powers from ICRU Report 35, the same used in TG-21. The discrepancy between measured data and EGS4 results could be due to the photon spectra used in this work. Although the type of accelerator modeled at NRC to produce the photon spectra was the same as that one used in the present work, the x-ray spectra may differ, so one can expect

that the percent depth dose determined with EGS4 may be slightly different than the measured data.

Two monoenergetic electron beams, 16 and 20 MeV were used in EGS4 code to predict the depth dose. The EGS4 electron depth dose curves in the water phantom were determined using incident broad parallel beams of monoenergetic electrons passing through 100 cm of air. The uncertainties affecting the EGS4 calculations are approximately 0.2% for both electron beam energies. The results are shown in Fig.3.5 and Fig.3.6. For both electron beams, in the peak region, the EGS4 and the measured percent depth doses differ by less than 2%.

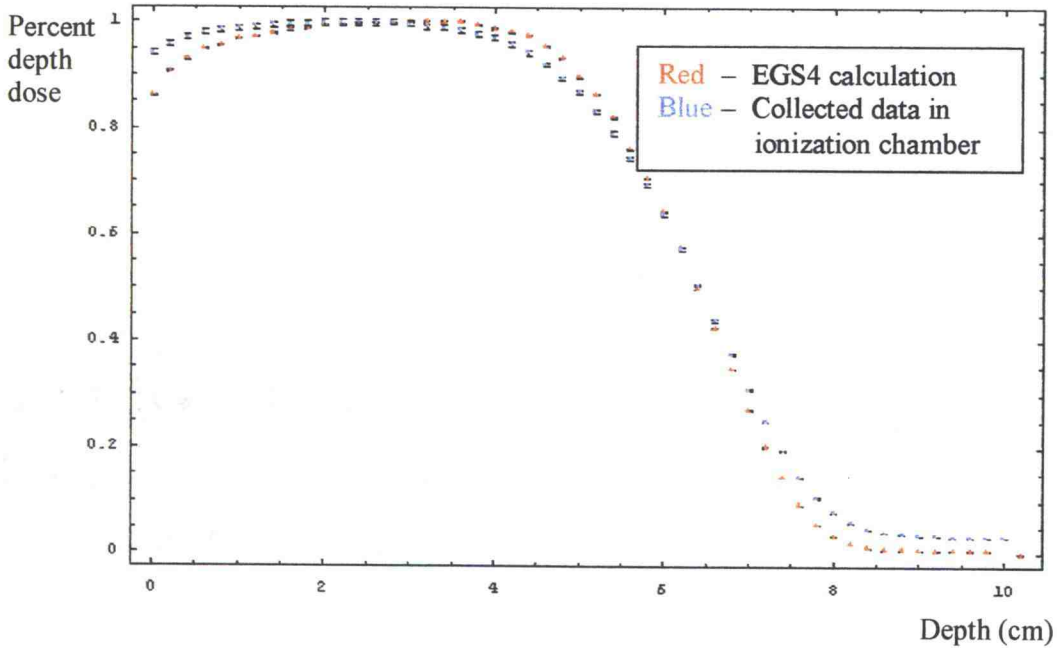

Figure 3.5. Comparison between EGS4 and measured percent depth dose for a 16 MeV energy electron beam.

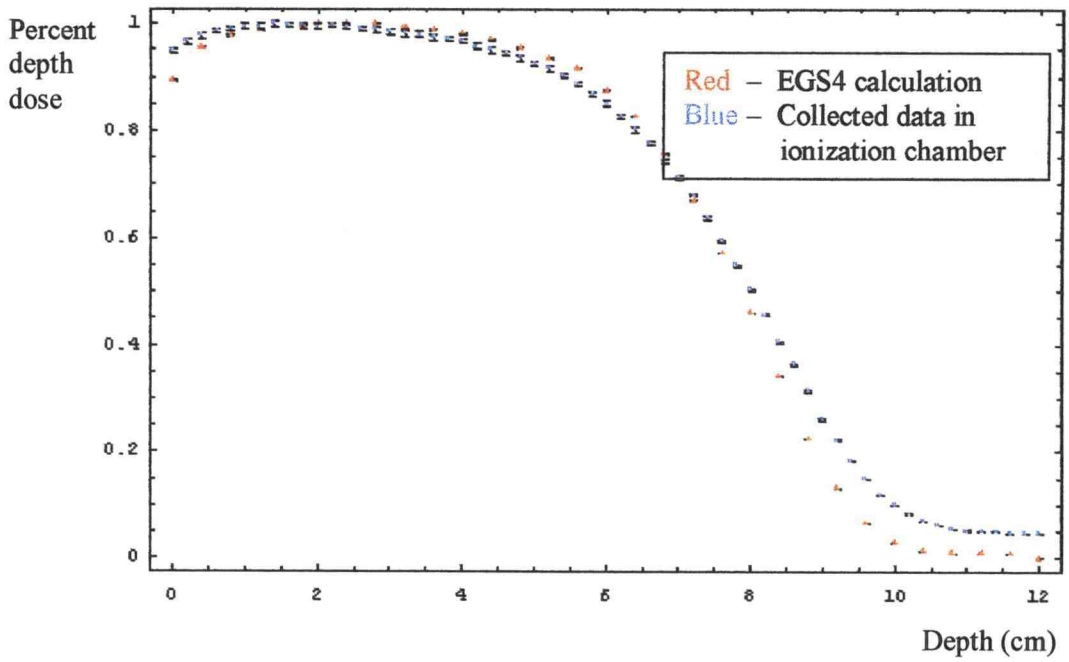

Figure 3.6. Comparison between EGS4 and measured percent depth dose for a 20 MeV energy electron beam

Compared with the corresponding measured data, the EGS4 results underestimate the dose near the surface and predict a steeper fall-off beyond d_{max}. The discrepancy between experimental and theoretical data can be explained by the neglect the spectrum of electrons and photon contamination, especially at higher energies where the radiative yield increases. The effect of contaminant photons in electron beams is to increase the stopping power ratios in the therapeutic range. The percent depth dose increases due to the contaminant photons.

4. CONCLUSIONS

In this work measurements of absorbed dose-to-water for 6 and 18 MV energy photon beams, and 16 and 20 MeV energy electron beams have been performed, using Capitec PR-06G and Capitec-05 cylindrical ionization chambers and a Varian Clinac 2100 C linear accelerator. Because the depths of calibration recommended in the TG-21 protocol differ from those recommended in the TG-51 protocol, to compare the absorbed dose-to-water determined according to the two protocols, d_{max} was chosen as a comparison depth.

Absorbed doses determined according to the TG-51 protocol were found to be higher than those determined with the TG-21 protocol. For photon beams with energies of 6 and 18 MV, the discrepancies are 1.4% and 1.7%, respectively, whereas for electron beams with energies 16 and 20 MeV, they are 1.8 % and 2.4%, respectively.

The measured ratios $\frac{D^{TG-51}}{D^{TG-21}}$ are compared with calculated ratios $\frac{D_{w,Q}^{TG-51}}{\left(D_{w,Q}^{TG-51}\right)_{data}^{TG-21}}$ based on TG-51 equations but calculating k_Q and $N_{D,w}^{^{60}Co}$ using TG-21 data. The discrepancies are found to be approximately 0.3% for both photon energies, and 0.7% and 0.6% for electron beams with energies of 16 and 20 MeV, respectively. The reasons for these discrepancies are the differences between the calibration procedures and the beam quality specifiers.

The TG-51 protocol is based on an absorbed dose-to-water calibration factor, while the TG-21 protocol relies on an exposure calibration factor. The differences between the calibration standards used by the two protocols lead to a difference of 2.2% between the measured and calculated values of $\frac{N_{D,w}^{^{60}Co}}{N_{gas}}$. The changes in beam quality specifiers lead to 0.4% and 0.8% for 6 and 18 MV energy photon beams, respectively. For electrons the differences are 0.3% and 0.8% for 16 and 20 MeV energy electron beams, respectively. The TG-21 protocol uses stopping powers for photons from ICRU Report 35 and for electrons from ICRU Report 37. The TG-51 protocol uses for both photons and electrons

stopping powers from ICRU Report 37. The change from exposure to absorbed dose-to-water calibrated ionization chambers has the strongest impact on the differences between TG-21 and TG-51 absorbed dose-to-water, while the change in beam quality specifier and stopping power ratios have only a very small effect on these differences.

The TG-51 protocol is very simple, minimizing the likelihood of error, because it starts with an absorbed dose-to-water calibration, while the TG-21 is very complex, starting with the calibration for exposure, which is different from the absorbed dose-to-water, the clinical quantity of interest. The TG-51 protocol allows the determination of a more accurate absorbed dose in a ^{60}Co beam than the TG-21 protocol since it uses a directly measured absorbed dose-to-water calibration factor, while the exposure based dosimetry system is dependent on external physical data which are not measured or controlled in clinics.

5. FUTURE WORK

One limitation of the Monte Carlo calculations performed in this work was that the radiation source monoenergetic electron beams and photon spectra were obtained at the National Research Council of Canada by simulation of a Varian Clinac 2100 C. Although the type of accelerator modeled at NRC was the same as that used in the present work, the spectra may differ. Another limitation is the small number of percent depth dose measurements in photon beams.

Recommended future work would be for more measurements in photon beams and the head of the accelerator modeled in EGS4 based on Varian detailed schematics. After checking the model against measured data used as benchmark, the photon and electron spectra obtained by accelerator head modeling could be used to provide an accurate description of the energy deposition inside an anthropomorphic female phantom. The female phantom (Figure 5.1) is based entirely on the mathematical models developed at Oak Ridge National Laboratory (Cristy et al 1987)

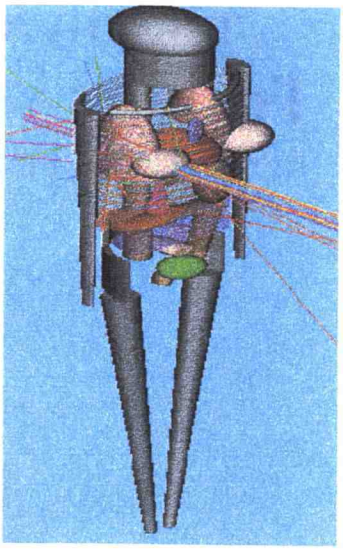

Figure 5.1. ORNL Female anthropomorphic phantom. The lines represent particle tracks visualized with Sabrina (Van Riper 1997)

BIBLIOGRAPHY

AAPM-American Association of Medical Physics TG-21, "A Protocol for the Determination of Absorbed Dose from High-Energy Photon and Electron Beams", Med. Phys. 10(6), 741-771 (1983)

AAPM-American Association of Medical Physics TG-51, "A Protocol for Clinical Reference Dosimetry of High-Energy Photon and Electron Beams", Med. Phys. 26(9), 1847-1870 (1999)

ACS-American Cancer Society, "Cancer Facts and Figures of 2002", www.cancer.org/ (2001)

Attix, F.H., "Introduction to Radiological Physics and Radiation Dosimetry", Wiley, New York (1986)

Burns, D.T. , Ding, G.X. and Rogers, D.W.O. , "R_{50} as a Beam Quality Specifier for Selecting Stopping Power Ratios and Reference Depths for Electron Dosimetry", Med. Phys. 23, 383-388 (1996)

Campbell, N.A., Reece, J.B., Mitchell, L., G., "Biology", Addison Wesley Logman, Inc., Menlo Park, California (1999)

Cho, S.H., Lowenstein, J.R., Balter, P.A., Wells, N.H. and Hanson, W.F., "Comparison Between TG-51 and TG-21: Calibration of Photon and Electron Beams in Water Using Cylindrical Chambers", Am. Coll. Med. Phys. 1(3), 108-115 (2000)

Cristy, M. and Eckerman, K.F., "Specific Absorbed Fractions of Energy at Various Ages From Internal Photon Sources", Oak Ridge National Laboratory Report ORNL/TM-8381/V1-V7 (1987)

Ding, G.X., Cygler, J.E., Kwok, C.B., "Clinical Reference Dosimetry: Comparison Between AAPM TG-21 and TG-51 Protocols", Med. Phys. 27(6), 1217-1225 (2000)

EGS4, "Monte Carlo Simulation of the Coupled Transport of Electrons and Photons", Radiation Safety Information Computational Center (RSICC), Oak Ridge National Laboratory, http://www-rsicc.ornl.gov/rsic.html (1985)

Hall, E.J., "Radiobiology for the Radiologist", J.B. Lippincott Company, Philadelphia, Pennsylvania (1994)

Huq, M.S. and Andreo, P., "Reference Dosimetry In Clinical High-Energy Photons Beams: Comparison of the AAPM TG-51 and AAPM TG-21 Dosimetry Protocols" Med. Phys. 28(1), 46-54 (2001)

Huq, M.S. and Song, H., "Reference Dosimetry In Clinical High-Energy Electrons Beams: Comparison of the AAPM TG-51 and AAPM TG-21 Dosimetry Protocols" Med. Phys. 28(10) 2077-2086 (2001)

ICRU, "Radiation Dosimetry: Electron Beams with Energies Between 1-50 MeV", Report 35, International Commission on Radiation Units and Measurements, Washington D.C. (1984)

ICRU, "Stopping Powers for Electrons and Positrons", Report 37, International Commission on Radiation Units and Measurements, Washington D.C. (1984)

Johns, H.E. and Cunningham, J.R., " The Physics of Radiology" 4th Ed, Charles C. Thomas, Springfield Illinois (1983)

Khan, F. M., "The Physics of Radiation Therapy", Williams & Wilkins, Baltimore MD (1984)

Kosunen, A. and Rogers, D.W.O., "Beam Quality Specification for Photon Beam Dosimetry", Med. Phys. 20, 1181-1188 (1993)

Li, X.A. and Rogers, D.W.O., "Reducing Electron Contamination for Photon Beam-Quality Specification", Med. Phys. 21, 791-798 (1994)

Mackie, R University of Wisconsin-Madison Medical School Comprehensive Cancer Center Web-based Educational Module for the Neoplasia Course On-Line, http://www.radiotherapy.wisc.edu/, (1997)

Pusey, W.A., "Roentgen –Rays in the Treatment of Skin Disease and for Removal of Hair", J.Cutan Genito-Urin Dis. July1900:18 302-315. (http://archderm.ama-assn.org/issues/v136n7/ffull/dac9007-1.html)

Rogers, D.W.O., Mackie, T.R., "BEAM: A Monte Carlo Code to Simulate Radiotherapy Treatment Units", Med. Phys. 22, 503-524 (1995)

Rogers, D.W.O, "Fundamenatls of Dosimetry Based on Absorbed Dose Standards", AAPM -Teletherapy Physics, present and Future, edited by Palta and Mackie 319-356 (1996)

Rogers, D.W.O, "A New Approach to Electron-Beam Reference Dosimetry", Med. Phys. 25, 310-320 (1998)

Rogers, D.O.W., "Correcting for Electron Contamination at Dose Maximum in Photon Beams", Med. Phys. 26(4), 533-537 (1999)

Rogers, D.O.W., "Corrected Relationship Between %dd(10)$_x$ and Stopping Power Ratios", Med. Phys. 26, 538-540 (1999)

Ross, G.M. "Induction of Cell Death by Radiotherapy, Endocrine –Related Cancer 6, 41-44 (1999), Online version via http://www.endocrinology.org

Spencer, L.V.and Attix, F.H., "A Theory of Cavity Ionization", Rad. Res. 3, 239-254 (1955)

Van Riper, K.A., "Sabrina User's Guide", White Rock Science (1997)

Varian Medical Systems (1999-2002), http://www.varian.com/onc/prd055.html

Wambersie, A. and Gahbauer, R.A., "Medical Applications of Electron Linacs", XVIII International Linac Conference 26-30 August 1996, Geneva, Switzerland (http://linac96.web.cern.ch/Linac96/Conference/Speakers.html)

Weinhous, M.S. and Meli, J.A., "Determining P_{ion}, the Correction Factor for Recombination Loses in an Ionization Chamber", Med. Phys. 11, 846-849 (1984)

APPENDICES

A. REPORT OF ABSORBED DOSE-TO WATER CALIBRATION OF CAPINTEC PR-06G IONIZATION CHAMBER

Report No. ADW0369

University of Wisconsin - Madison
Department of Medical Physics
Accredited Dosimetry Calibration Laboratory

1530 Medical Sciences Center, 1300 University Ave., Madison, WI 53706
Office (608) 262-6320 Fax: (608) 262-5012

Report of Absorbed Dose to Water Calibration for

Ionization Chamber

Submitted by: Thomas M. Potts, M.S.
Regional Cancer Center
Good Samaritan Hospital
3600 NW Samaritan Dr.
Corvallis, OR 97330

Ion Chamber: Capintec
Model PR-06G
S/N CII.6G8747

Date Received: 29/FEB/2000 Calibration Completed: 1/MAR/2000

Report No. **ADW0369**

University of Wisconsin - Madison
Department of Medical Physics
Accredited Dosimetry Calibration Laboratory

Cobalt-60 Absorbed Dose Measurement Data

Calibration Completed: March 1, 2000

Report Date: March 1, 2000

Ionization Chamber
Capintec
Model PR-06G

Serial Number : CII.6G8747
Nominal Volume : 0.6 cm^3
Type : Farmer

Electrometer used in Calibration
Standard Imaging, Inc. Model Max 4000

Serial Number : E992941
Scale : Std pC

Field Size	:	10 cm x 10 cm at 100 cm Source-Chamber Distance
Depth in Water	:	5 cm
Chamber Orientation	:	Serial Number toward beam
Chamber Reference Point	:	Center of chamber volume
Collecting Electrode Bias	:	+300 V
Charge Collected	:	Negative
Pre-Irradiation Leakage	:	-4.3×10^{-15} A
Calibration Classification	:	II
Ion Collection Efficiency (A_{ion})	:	0.9988 .

Beam Quality	Absorbed Dose to Water Rate (mGy/s)	Absorbed Dose to Water Calibration Factor $N_{D,w}$ (Gy/C)	Sleeve
Co-W	14.06	5.008×10^7	UW-ADCL 1.0 mm PMMA

Comments: The reported calibration factors have been corrected to 22° C and 760 Torr for 100% ion collection efficiency. Please refer to the appendix for a complete description of reported calibration factors.

Recorded in data book: ADW-02

Page: 183

Calibrated by: Daniel R. Anderson, M.S.
Staff Physicist
Accredited Dosimetry Calibration Laboratory

Reviewed by: T. Rockwell Mackie, Ph.D.
Vice Chairman
UW-ADCL Advisory Committee

B. REPORT OF EXPOSURE CALIBRATION OF CAPINTEC PR-06G IONIZATION CHAMBER

Report No. **ION6100**

University of Wisconsin - Madison
Department of Medical Physics
Accredited Dosimetry Calibration Laboratory

1530 Medical Sciences Center, 1300 University Ave., Madison, WI 53706
Office (608) 262-6320 Fax: (608) 262-5012

Report of Calibration for

Ionization Chamber

Submitted by: Thomas M. Potts, M.S.
Regional Cancer Center
Good Samaritan Hospital
3600 NW Samaritan Dr.
Corvallis, OR 97330

Ion Chamber: Capintec
Model PR-06G
S/N CII.6G8747

Date Received: 29/FEB/2000 Calibration Completed: 17/MAR/2000

University of Wisconsin - Madison
Department of Medical Physics
Accredited Dosimetry Calibration Laboratory

Cobalt-60 Measurement Data

Calibration Completed: March 2, 2000

Report Date: March 17, 2000

Ionization Chamber
Capintec
Model PR-06G

Serial Number : CII.6G8747
Nominal Volume : 0.6 cm^3
Type : Farmer

Electrometer used in Calibration
Standard Imaging, Inc. Model Max 4000

Serial Number : E992941
Scale : Std pC

Field Size	:	10 cm x 10 cm at 100 cm Source-Chamber Distance
Chamber Orientation	:	Serial Number toward beam
Chamber Reference Point	:	Center of chamber volume
Collecting Electrode Bias	:	+300 V
Charge Collected	:	Negative
Pre-Irradiation Leakage	:	-6.7×10^{-15} A
Calibration Classification	:	I
Ion Collection Efficiency (A_{ion})	:	0.999

Beam Quality	Air Kerma Rate (mGy/s)	Air Kerma Calibration Factor (Gy/C)	Exposure Calibration Factor (R/C)	Buildup Material
Co-60	13.57	4.547×10^7	5.173×10^9	Polystyrene

Comments: The reported calibration factors have been corrected to 22°C and 760 mm mercury. Please refer to the appendix for a complete description of reported calibration factors.

Recorded in data book: CO-20 Page: 173

Calibrated by: Daniel R. Anderson, M.S.
Staff Physicist
Accredited Dosimetry Calibration Laboratory

Reviewed by: T. Rockwell Mackie, Ph.D.
Vice Chairman
UW-ADCL Advisory Committee

C. DESCRIPTION OF CAPINTEC PR-06G IONIZATION CHAMBER

PR-06C , PR-06G

0.6 mℓ

Air Equivalent Plastic

Farmer Replacement Ionization Chamber

This ionization chamber probe is suitable for therapeutic grade calibrations and measurements of radiation fields in clinical applications. The probe is very precise, stable and highly reliable, yet it is very rugged and able to withstand rough handling.

The outer dimensions of this probe are the same as that of the Farmer Secondary Standard Ionization Chamber. The energy response of this probe is the same as, or exceeds that of the Farmer Chamber in all respects. A Farmer Chamber can therefore, be replaced by this Capintec 0.6 mℓ Ionization Chamber with the added advantage of superior characteristics and ruggedness.

Applications

Therapeutic Level Calibrations and Measurements in Air and in Phantoms

Superficial, Orthovoltage x-rays,
Cs, Ra, Co γ-rays,
Linear Accelerator, Betatron Beams,
Dose Calibration, Output Calibration,
Depth Dose Measurement, Iso-Dose Plots,
Beam Flatness Confirmation,
Entrance/Exit Dose Rate,
Intracavitary (rectum, uterus) Dose Study,
Diagnostic x-ray System Calibrations
and Measurements in Air,
HVL Measurements.

Specifications

Type of Chamber:	Air Equivalent Ionization Cavity, Coaxial.
Sensitivity:	0.200 nC/R typical.
Maximum Display:	2000 R, R/min (with Model 192).
Maximum Resolution:	0.001 R, R/min (with Model 192).
Energy Response:	±2% (for Range II, measured in air without build-up cap),

	±1% (for Range III, measured in air with build-up cap),
	±2% (for Range IV, in phantom, calculated),
	±1.5% (for Range IV, measured in phantom, with respect to Farmer Secondary Standard Chamber normalized at ^{60}Co).
Stability:	Within ±0.3% (observed by using ^{60}Co beam, for over a two year period).
Stem Effect:	Less than ±0.5% (for 0.3m x 0.3m field).
Leakage Current:	Less than 10^{-14}A (nominal).
Polarization Time Required:	Five minutes typical (depends upon previous voltage).
Beam Soaking Time Required:	Two minutes typical.
Beam Rate Dependency:	28 kR/min for continuous beam, 40 mR/pulse for pulsed beam, (0.5% collection loss, with 300 Volts).
Beam Direction:	Primary beam perpendicular to the chamber axis.
Ion Transit Time:	0.14 msec
Chamber Material:	Air Equivalent Plastic ~ C552
Volume:	0.65 mℓ
Diameter:	7.0 mm
Length:	22 mm
Wall Thickness:	0.28 mm, 50 mg/cm^2
Stem Diameter:	8.6 mm
Cable Length:	2 meter (PR-06G)
Connector:	BNC Size Male Triaxial.

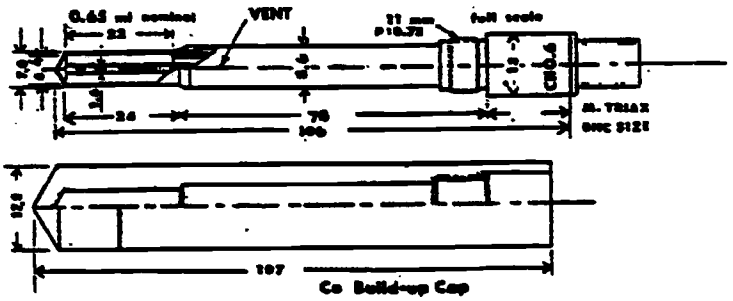
VENT
24
70
197
Co Build-up Cap

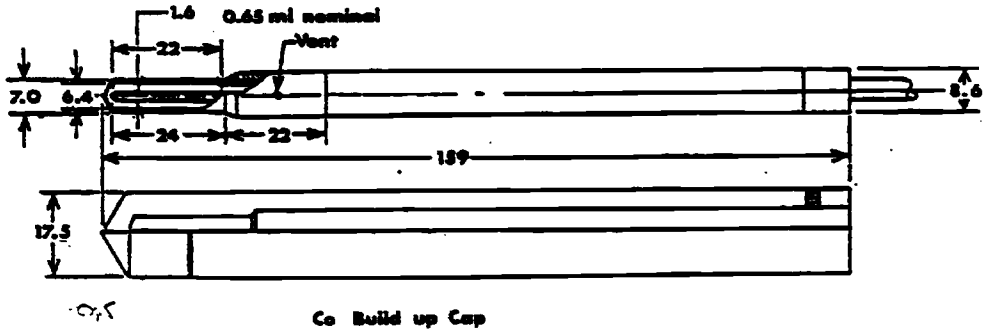
1.6
0.65 ml nominal
22
Vent
7.0
6.4
8.6
24
22
159
17.5
Co Build up Cap

D. DESCRIPTION OF CAPINTEC PR-05 IONIZATION CHAMBER

PR-05, (PR-05P)

0.14 mℓ (0.07 mℓ)

Air Equivalent Plastic

Mini-Chamber (Intracavitary Chamber)

This ionization chamber is suitable for therapeutic level measurements of radiation fields in clinical and in industrial applications. The sensitive volume of this chamber is very small and the outer shape is rather simple. The chamber may therefore, be used as a detector for depth dose and iso-dose studies in a water phantom where good spatial resolution and high dose rate measurements are essential. The microphonic noise level of this chamber assembly is very low.

This probe has been shown to be a very useful tool for determining intracavitary doses, where measurements of low dose rates are necessary.

The chamber is available in two volume sizes, 0.14 mℓ (PR-05) and 0.07 mℓ (PR-05P). The geometries of both size chambers are identical except for the cavity length. The attainable display resolution of a Model 192 with a 0.07 mℓ chamber is 0.01 R and R/min, whereas a Model 192 can be set for the maximum display resolution of either 0.001 R, R/min or 0.01 R, R/min when a 0.14 mℓ chamber is used.

Applications

Therapeutic Measurements in Phantoms and in Cavities

Linear Accelerator and Betatron Beams,
Cs, Ra, Co, and etc. γ-rays,
Orthovoltage x-rays.

Specifications

Sensitivity:	0.042 nC/R typical for PR-05, 0.021 nC/R typical for PR-05P.
Maximum Display:	2000 R, R/min (direct reading), over 40 kR, kR/min by using electrometer position of Model 192.
Maximum Resolution:	0.001 R, R/min for PR-05, 0.01 R, R/min for PR-05P (with Model 192).
Energy Response:	±3% (for Range II, measured in air without build-up cap),

	±1% (for Range III, measured in air with build-up cap),
	±2% (for Range IV, in phantom, calculated).
Stability:	Within ±0.5% (for one year).
Stem Effect:	Less than ±1%.
Leakage Current:	Less than 10^{-14}A (nominal).
Polarization Time Required:	Five minutes typical (depends upon previous voltage).
Beam Soaking Time Required:	One minute typical.
Beam Rate Dependency:	150 kR/min for continuous beam, 95 mR/pulse for pulsed beam, (0.5% collection loss, with 300 Volts).
Beam Direction:	Primary beam perpendicular to the chamber axis.
Ion Transit Time:	0.06 msec
Chamber Material:	Air Equivalent Plastic
Volume:	0.14 mℓ (PR-05), 0.07 mℓ (PR-05P)
Diameter:	6.4 mm
Length:	11.5 mm (PR-05), 5.5 mm (PR-05P)
Wall Thickness:	1.2 mm, 0.22 g/cm^2
Cable and Connector:	Capintec Low Noise Triaxial Cable, 2.5 m long typical, with BNC Size Male Triaxial Connector.

CAUTION: *All the Capintec Ionization Chamber Probes are ventilated to the atmosphere. Be sure to use a proper protecting cover.*

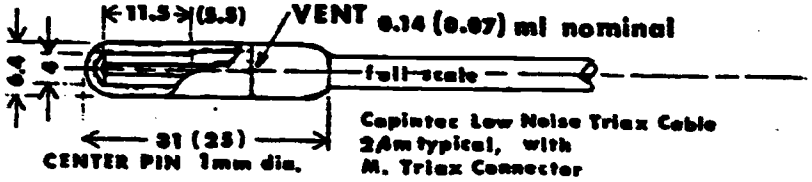
11.5 (3.5)
VENT 0.14 (0.07) ml nominal
full-scale
31 (25)
CENTER PIN 1mm dia.
Capintec Low Noise Triax Cable
2.5m typical, with
M. Triax Connector

E. REALISTIC 6 AND 18 MV ENERGY PHOTON SPECTRA OBTAINED AT NATIONAL RESEARCH COUNCIL OF CANADA BY MODELING A VARIAN CLINAC 2100 C LINEAR ACCELERATOR USING BEAM CODE

E.1. 6 MV PHOTON BEAM

Photon Energy (MeV)	Relative number per energy interval	Photon Energy (MeV)	Relative number per energy interval
0.00000	0	3.750E+00	1.4005E-06
2.500E-01	9.4485E-06	4.000E+00	1.2077E-06
5.000E-01	9.5786E-06	4.250E+00	1.0442E-06
7.500E-01	8.0766E-06	4.500E+00	8.6051E-07
1.000E+00	6.8650E-06	4.750E+00	7.4537E-07
1.250E+00	5.8836E-06	5.000E+00	5.7857E-07
1.500E+00	5.0212E-06	5.250E+00	4.3973E-07
1.750E+00	4.2913E-06	5.500E+00	2.8741E-07
2.000E+00	3.7020E-06	5.750E+00	1.2629E-07
2.250E+00	3.2493E-06	6.000E+00	7.6060E-09
2.500E+00	2.7831E-06	6.250E+00	7.6060E-19
2.750E+00	2.4103E-06	6.500E+00	7.6060E-19
3.000E+00	2.1283E-06	6.750E+00	7.6060E-19
3.250E+00	1.8404E-06	7.000E+00	7.6060E-24
3.500E+00	1.5743E-06		

E.2. 18 MV PHOTON BEAM

Photon Energy (MeV)	Relative number per energy interval
0.00000	0
2.500E-01	4.0337E-06
5.000E-01	9.5959E-06
7.500E-01	1.2065E-05
1.000E+00	1.3781E-05
1.250E+00	1.4319E-05
1.500E+00	1.4062E-05
1.750E+00	1.3924E-05
2.000E+00	1.3086E-05
2.250E+00	1.2041E-05
2.500E+00	1.1453E-05
2.750E+00	1.0889E-05
3.000E+00	1.0112E-05
3.250E+00	9.3359E-06
3.500E+00	8.7616E-06
3.750E+00	8.1366E-06
4.000E+00	7.6597E-06
4.250E+00	7.1010E-06
4.500E+00	6.7447E-06
4.750E+00	6.2360E-06
5.000E+00	5.8474E-06
5.250E+00	5.4393E-06
5.500E+00	5.2179E-06
5.750E+00	4.8653E-06
6.000E+00	4.6058E-06
6.250E+00	4.2906E-06
6.500E+00	4.0800E-06
6.750E+00	3.8501E-06
7.000E+00	3.6913E-06
7.250E+00	3.6273E-06
7.500E+00	3.2497E-06
7.750E+00	3.1424E-06
8.000E+00	2.8892E-06
8.250E+00	2.8118E-06
8.500E+00	2.6369E-06
8.750E+00	2.5523E-06
9.000E+00	2.3753E-06
9.250E+00	2.2205E-06
9.500E+00	2.1544E-06
9.750E+00	2.0812E-06
1.000E+01	2.0213E-06
1.025E+01	1.9223E-06
1.050E+01	1.7353E-06
1.075E+01	1.7610E-06
1.100E+01	1.6670E-06
1.125E+01	1.5800E-06
1.150E+01	1.4863E-06
1.175E+01	1.3896E-06
1.200E+01	1.4569E-06
1.225E+01	1.2893E-06
1.250E+01	1.2828E-06
1.275E+01	1.1637E-06
1.300E+01	1.0773E-06
1.325E+01	1.0395E-06
1.350E+01	1.0556E-06
1.375E+01	9.6263E-07
1.400E+01	9.1664E-07
1.425E+01	8.9720E-07
1.450E+01	8.7556E-07
1.475E+01	7.7567E-07
1.500E+01	7.4345E-07
1.525E+01	6.8121E-07
1.550E+01	6.3706E-07
1.575E+01	5.4163E-07
1.600E+01	5.6762E-07
1.625E+01	4.8476E-07
1.650E+01	4.3953E-07
1.675E+01	4.0895E-07
1.700E+01	3.2791E-07
1.725E+01	2.8358E-07
1.750E+01	2.1152E-07
1.775E+01	1.3752E-07
1.800E+01	6.5072E-08
1.825E+01	6.5072E-13

F. MEASURED DATA AND DOSE CALCULATION

F.1. TG-21 – 6 MV PHOTON BEAM

a. Determination of ionization ratio and related quantities

SAD=100 cm

Field size: 10x10 cm^2

V=+300 V

Time=200 MU

Chamber model: Capintec PR-06G

Wall material: C552

Inner diameter: 6.4 mm

d=20 cm $Q_{20,avg}$=-20.955 nC

d=10 cm $Q_{10,avg}$=-31.720 nC

$$TPR_{10}^{20} = \frac{Q_{20,avg}}{Q_{10,avg}} = 0.661$$

FIG.3 of (AAPM 1983): Nominal Potential= 4.4 V

FIG.5 of (AAPM 1983): P_{repl}=0.992

FIG.7 of (AAPM 1983): α=0.26

TABLE IX of (AAPM 1983): $\left(\frac{\mu}{\rho}\right)_{C552}^{water} = 1.111$

FIG.2 or TABLE IV of (AAPM 1983): $\left(\frac{L}{\rho}\right)_{air}^{water} = 1.129$

$\left(\frac{L}{\rho}\right)_{air}^{C552} = 0.995$

EQ.(2-20): P_{wall}=0.995

b. Determination of P_{ion}

Chamber model: Capintec PR-06G

Wall material: C552

Inner diameter: 6.4 mm

SAD=100 cm

Time=200 MU

Field size: 10x10 cm^2

d=5 cm

V_1=+300 V $Q_{1,avg}$=-37.81 nC

V_2=+150 V $Q_{2,avg}$=-37.67 nC

$\frac{Q_{1,avg}}{Q_{2,avg}}$ =1.0037

FIG.4 of (AAPM 1983): P_{ion}=1.004

c. Determination of dose-to-water per monitor unit

Chamber model: Capintec PR-06G

Wall material: C552

Inner diameter: 6.4 mm

SAD=100 cm

Time=200 MU

Field size: 10x10 cm^2

d=5 cm

V=+300 V

p=764.44 torr

t=15.0 °C

TMR=0.921

Sleeve correction Factor=1.004

Q_{avg}=-38.033 nC

Dose to water/MU at d_{max}:

$\dot{D}_{TG-21}^{6MV} = 0.990 cGy/MU$

F.2. TG-51 – 6 MV PHOTON BEAM

a. Determination of k_Q and related quantities

SSD=100 cm

Field size: 10x10 cm^2

V=+300 V

Time=200 MU

Chamber model: Capintec PR-05

Wall material: C552

Inner diameter: 2 mm

d=10.12 cm $Q_{10,avg}$=-5.653 nC

d=1.62 cm $Q_{1.5,avg}$=-8.581 nC

$$\%dd(10)_x = \%dd(10) = 65.88$$

TABLE I of (AAPM 1999): k_Q=0.994

b. Determination of P_{ion}

Chamber model: Capintec PR-06G

Wall material: C552

Inner diameter: 6.4 mm

SAD=100 cm

Time=200 MU

Field size: 10x10 cm^2

d=10 cm

V_1=+300 V $Q_{1,avg}$=-31.393 nC

V_2=+150 V $Q_{2,avg}$=-31.303 nC

EQ.(2-31): P_{ion}=1.003

c. Determination of P_{pol}

Chamber model: Capintec PR-06G

Wall material: C552

Inner diameter: 6.4 mm

SAD=100 cm

Time=200 MU

Field size: 10x10 cm^2

d=10 cm

V_1=+300 V $Q_{1,avg}$=-31.393 nC

V_2=-300 V $Q_{2,avg}$=31.435 nC

EQ.(2-32) P_{pol}=1.0007

d. Determination of dose-to-water per monitor unit

Chamber model: Capintec PR-06G

Wall material: C552

Inner diameter: 6.4 mm

SAD=100 cm

Time=200 MU

Field size: 10x10 cm^2

d=10 cm

V=+300 V

p=764.44 torr

t=15.0 °C

TMR=0.773

$Q_{,avg}$=-32.02 nC

Dose to water/MU at d_{max}:

$$\dot{D}^{6MV}_{TG-51} = 1.004 cGy/MU$$

F.3. TG-21 – 18 MV PHOTON BEAM

a. Determination of ionization ratio and related quantities

SAD=100 cm

Field size: 10x10 cm^2

V=+300 V

Time=200 MU

Chamber model: Capintec PR-06G

Wall material: C552

Inner diameter: 6.4 mm

d=20 cm $Q_{20,avg}$=-29.647 nC

d=10 cm $Q_{10,avg}$=-37.783 nC

$$TPR_{10}^{20} = \frac{Q_{20,avg}}{Q_{10,avg}} = 0.785$$

FIG.3 of (AAPM 1983): Nominal Potential= 16.82 V

FIG.5 of (AAPM 1983): P_{repl}=0.994

FIG.7 of (AAPM 1983): α=0.125

TABLE IX of (AAPM 1983): $\left(\frac{\mu}{\rho}\right)_{C552}^{water} = 1.108$

FIG.2 or TABLE IV of (AAPM 1983): $\left(\frac{L}{\rho}\right)_{air}^{water} = 1.102$

$\left(\frac{L}{\rho}\right)_{air}^{C552} = 0.969$

EQ.(2-20): P_{wall}=0.997

b. Determination of P_{ion}

Chamber model: Capintec PR-06G

Wall material: C552

Inner diameter: 6.4 mm

SAD=100 cm

Time=200 MU

Field size: 10x10 cm^2

d=7 cm

V_1=+300 V $Q_{1,avg}$=-40.197 nC

V_2=+150 V $Q_{2,avg}$=-39.907nC

$\frac{Q_{1,avg}}{Q_{2,avg}}$ =1.0073

FIG.4 of (AAPM 1983): P_{ion}=1.007

c. Determination of dose-to-water per monitor unit

Chamber model: Capintec PR-06G

Wall material: C552

Inner diameter: 6.4 mm

SAD=100 cm

Time=200 MU

Field size: 10x10 cm^2

d=7 cm

V=+300 V

p=752.13 torr

t=22.0 °C

TMR=0.961

Sleeve correction Factor=1.007

Q_{avg}=-38.83 nC

Dose to water/MU at d_{max}:

$D_{TG-21}^{18MV} = 0.994cGy/MU$

F.4. TG-51 – 18 MV PHOTON BEAM

a. Determination of k_Q and related quantities

SSD=100 cm

Field size: 10x10 cm^2

V=+300 V

Time=200 MU

Chamber model: Capintec PR-05

Wall material: C552

Inner diameter: 2 mm

1 mm lead placed at 29 cm

d=10.12 cm $Q_{10,avg}$=--6.220 nC

d=3.12 cm $Q_{1.5,avg}$=--7.771 nC

$\%dd(10)_{Pb} = 80.0 \rightarrow \%dd(10)_x = 81.8$

TABLE I of (AAPM 1999): k_Q=0.97

b. Determination of P_{ion}

Chamber model: Capintec PR-06G

Wall material: C552

Inner diameter: 6.4 mm

SAD=100 cm

Time=200 MU

Field size: 10x10 cm^2

d=10 cm

V_1=+300 V $Q_{1,avg}$=-36.887 nC

V_2=+150 V $Q_{2,avg}$=-31.68 nC

EQ.(2-31): P_{ion}=1.0057

c. Determination of P_{pol}

Chamber model: Capintec PR-06G

Wall material: C552

Inner diameter: 6.4 mm

SAD=100 cm

Time=200 MU

Field size: 10x10 cm^2

d=10 cm

V_1=+300 V $Q_{1,avg}$=-36.887 nC

V_2=-300 V $Q_{2,avg}$=36.95 nC

EQ.(2-32) P_{pol}=1.00085

d. Determination of dose-to-water per monitor unit

Chamber model: Capintec PR-06G

Wall material: C552

Inner diameter: 6.4 mm

SAD=100 cm

Time=200 MU

Field size: 10x10 cm^2

d=10 cm

V=+300 V

p=752.13 torr

t=22.0 °C

TMR=0.908

$Q_{,avg}$=-36.887 nC

Dose to water/MU at d_{max}:

$$\dot{D}_{TG-51}^{18MV} = 1.011 cGy/MU$$

F.5. TG-21 – 16 MeV ELECTRON BEAM

a. Determination of mean incident energy and related quantities

SSD=100 cm

Field size: 15x15 cm^2

V=+300 V

Time=200 MU

Chamber model: Capintec PR-06G

Wall material: C552

Inner diameter: 6.4 mm

Using experimental data presented in Appendix 7, one plotted the percent depth dose (See Fig.3.1). Based on the graph one has determined:

I_{50}=6.42 cm

d_{max}=2.78 cm

R_P=7.826 cm

E_0=14.959 MeV

E_z=9.465 MeV

Table V of (AAPM 1983): $\left(\frac{L}{\rho}\right)_{air}^{water} = 1.012$

Table VIII of (AAPM 1983): P_{repl}=0.979

b. Determination of P_{ion}

Chamber model: Capintec PR-06G

Wall material: C552

Inner diameter: 6.4 mm

SSD=100 cm

Time=200 MU

Field size: 15x15 cm^2

d=3.3 cm

V_1=+300 V $Q_{1,avg}$=-45.63 nC

V_2=+150 V $Q_{2,avg}$=-45.23 nC

$\frac{Q_{1avg}}{Q_{2avg}}$ =1.0088

Fig.4 of (AAPM 1983): P_{ion}=1.01

c. Determination of dose-to-water per monitor unit

Chamber model: Capintec PR-06G

Wall material: C552

Inner diameter: 6.4 mm

SSD=100 cm

Time=200 MU

Field size15x15 cm^2

d=3.3 cm

V=+300 V

p=763.89 torr

t=21.0 °C

Sleeve correction Factor=1.004

Q_{avg}=-45.63 nC

Dose to water/MU at d_{max}:

$D_{TG-21}^{16MeV} = 0.998c/MU$

F.6. TG-51 – 16 MeV ELECTRON BEAM

a. Determination of electron quality conversion factor and related quantities

SSD=100 cm

Field size: 15x15 cm^2

V=+300 V

Time=200 MU

Chamber model: Capintec PR-06G

Wall material: C552

Inner diameter: 6.4 mm

Using experimental data presented in Appendix 7, one plotted the percent depth dose (See Fig.3.1). Based on the graph one has determined:

I_{50}=6.42 cm

d_{max}=2.78 cm

k_{ecal}=0.900

d_{ref}=3.83 cm

Fig.5 of (AAPM 1999): $k'_{R_{50}} = 1.002$

Eq.(2-36): $k_{R_{50}} = 0.9018$

d_{ref}=3.83 cm Q_1=-45.44 nC

$d_{ref}+0.5r_{cav}$=3.99 cm Q_2=-45.36 nC

Eq.(2-37): $P_{gr}^{Q} = 0.998$

Eq.(2-35): k_Q=0.899

b. Determination of P_{ion}

Chamber model: Capintec PR-06G

Wall material: C552

Inner diameter: 6.4 mm

SSD=100 cm

Time=200 MU

Field size: 15x15 cm^2

d=3.83 cm

V_1=+300 V $Q_{1,avg}$=-45.44 nC

V_2=+150 V $Q_{2,avg}$=-45.17 nC

Eq.(2-31): P_{ion}=1.006

c. Determination of P_{pol}

Chamber model: Capintec PR-06G

Wall material: C552

Inner diameter: 6.4 mm

SSD=100 cm

Time=200 MU

Field size: 15x15 cm^2

d=3.83 cm

V_1=+300 V $Q_{1,avg}$=-45.44 nC

V_2=-300 V $Q_{2,avg}$=45.55 nC

Eq.(2-32) P_{pol}=1.0012

d. Determination of dose to water per monitor unit

SSD=100 cm

Time=200 MU

Field size: 15x15 cm^2

d=3.83 cm

V=+300 V

p=763.89 torr

t=21.0 °C

Q_{avg}=-45.44 nC

%dd=0.995

Dose to water/MU at d_{max}:

$$\dot{D}_{TG-51}^{16MeV} = 1.016 cGy/MU$$

F.7. TG-21 – 20 MeV ELECTRON BEAM

a. Determination of mean incident energy and related quantities

SSD=100 cm

Field size: 15x15 cm^2

V=+300 V

Time=200 MU

Chamber model: Capintec PR-06G

Wall material: C552

Inner diameter: 6.4 mm

Using experimental data presented in Appendix 7, one plotted the percent depth dose (See Fig.3.2). Based on the graph one has determined:

I_{50}=8.02 cm

d_{max}=1.55 cm

R_P=9.953 cm

E_0=18.687 MeV

E_z=15.777 MeV

Table V of (AAPM 1983): $\left(\frac{L}{\rho}\right)_{air}^{water} = 0.975$

Table VIII of (AAPM 1983): P_{repl}=0.991

b. Determination of P_{ion}

Chamber model: Capintec PR-06G

Wall material: C552

Inner diameter: 6.4 mm

SSD=100 cm

Time=200 MU

Field size: 15x15 cm^2

d=2.0 cm

V_1=+300 V $Q_{1,avg}$=-46.61 nC

V_2=+150 V $Q_{2,avg}$=-46.22 nC

$\frac{Q_{1avg}}{Q_{2avg}}$ =1.0085

Fig.4 of (AAPM 1983): P_{ion}=1.01

c. Determination of dose-to-water per monitor unit

Chamber model: Capintec PR-06G

Wall material: C552

Inner diameter: 6.4 mm

SSD=100 cm

Time=200 MU

Field size15x15 cm^2

d=2.0 cm

V=+300 V

p=763.89 torr

t=21.0 °C

Sleeve correction Factor=1.002

Q_{avg}=-46.61 nC

Dose to water/MU at d_{max}:

$D_{TG\ 21}^{20MeV} = 0.994c/MU$

F.8. TG-51 – 20 MeV ELECTRON BEAM

a. Determination of electron quality conversion factor and related quantities

SSD=100 cm

Field size: 15x15 cm^2

V=+300 V

Time=200 MU

Chamber model: Capintec PR-06G

Wall material: C552

Inner diameter: 6.4 mm

Using experimental data presented in Appendix 7, one plotted the percent depth dose (See Fig.3.2). Based on the graph one has determined:

I_{50}=8.02 cm

d_{max}=1.55 cm

k_{ecal}=0.900

d_{ref}=4.814 cm

Fig.5 of (AAPM 1999): $k'_{R_{50}} = 0.998$

Eq.(2-36): $k_{R_{50}} = 0.8982$

d_{ref}=4.814 cm Q_1=-44.27 nC

$d_{ref}+0.5r_{cav}$=4.974 cm Q_2=-43.74 nC

Eq.(2-37): $P_{gr}^{Q} = 0.988$

Eq.(2-35): k_Q=0.887

b. Determination of P_{ion}

Chamber model: Capintec PR-06G

Wall material: C552

Inner diameter: 6.4 mm

SSD=100 cm

Time=200 MU

Field size: 15x15 cm^2

d=4.814 cm

V_1=+300 V $Q_{1,avg}$=-44.27 nC

V_2=+150 V $Q_{2,avg}$=-43.96 nC

Eq.(2-31): P_{ion}=1.0071

c. Determination of P_{pol}

Chamber model: Capintec PR-06G

Wall material: C552

Inner diameter: 6.4 mm

SSD=100 cm

Time=200 MU

Field size: 15x15 cm^2

d=4.814 cm

V_1=+300 V $Q_{1,avg}$=-44.27 nC

V_2=-300 V $Q_{2,avg}$=44.32 nC

Eq.(2-32) P_{pol}=1.0006

d. Determination of dose to water per monitor unit

SSD=100 cm

Time=200 MU

Field size: 15x15 cm^2

d=4.814 cm

V=+300 V

p=763.89 torr

t=21.0 °C

Q_{avg}=-44.27 nC

%dd=0.965

Dose to water/MU at d_{max}:

$$\dot{D}_{TG-51}^{20MeV} = 1.018 cGy/MU$$

G. MEASURED PERCENT DEPTH IONIZATION DATA FOR 16 AND 20 MeV ELECTRON BEAMS

G.1. 16 MeV ELECTRON BEAM

Depth	Percent depth dose	Depth	Percent depth dose
0.00	0.940	6.20	0.572
0.20	0.957	6.40	0.506
0.40	0.970	6.60	0.439
0.60	0.979	6.80	0.375
0.80	0.984	7.00	0.309
1.00	0.988	7.20	0.249
1.20	0.991	7.40	0.195
1.40	0.994	7.60	0.145
1.60	0.995	7.80	0.107
1.80	0.996	8.00	0.080
2.00	0.998	8.20	0.060
2.20	0.998	8.40	0.047
2.40	0.999	8.60	0.040
2.60	0.998	8.80	0.036
2.80	0.999	9.00	0.033
3.00	0.995	9.20	0.033
3.20	0.991	9.40	0.031
3.40	0.989	9.60	0.031
3.60	0.984	9.80	0.030
3.80	0.976	10.00	0.030
4.00	0.969	10.20	0.030
4.20	0.958	10.40	0.030
4.40	0.942	10.60	0.030
4.60	0.920	10.80	0.029
4.80	0.894	11.00	0.028
5.00	0.867	11.20	0.028
5.20	0.832	11.40	0.028
5.40	0.790	11.60	0.027
5.60	0.743	11.80	0.027
5.80	0.694		

G.2. 20 MeV ELECTRON BEAM

Depth	Percent depth dose	Depth	Percent depth dose
0.00	0.948	7.20	0.680
0.20	0.965	7.40	0.637
0.40	0.977	7.60	0.594
0.60	0.986	7.80	0.549
0.80	0.990	8.00	0.503
1.00	0.994	8.20	0.457
1.20	0.995	8.40	0.406
1.40	0.999	8.60	0.363
1.60	0.997	8.80	0.314
1.80	0.996	9.00	0.262
2.00	0.995	9.20	0.222
2.20	0.997	9.40	0.183
2.40	0.995	9.60	0.150
2.60	0.990	9.80	0.120
2.80	0.988	10.00	0.099
3.00	0.984	10.20	0.082
3.20	0.981	10.40	0.069
3.40	0.979	10.60	0.061
3.60	0.973	10.80	0.055
3.80	0.970	11.00	0.052
4.00	0.966	11.20	0.050
4.20	0.957	11.40	0.049
4.40	0.950	11.60	0.048
4.60	0.944	11.80	0.048
4.80	0.935	12.00	0.047
5.00	0.925	12.20	0.047
5.20	0.916	12.40	0.046
5.40	0.902	12.60	0.046
5.60	0.888	12.80	0.045
5.80	0.869	13.00	0.045
6.00	0.851	13.20	0.044
6.20	0.826	13.40	0.044
6.40	0.802	13.60	0.043
6.60	0.776	13.80	0.043
6.80	0.742	14.00	0.042
7.00	0.712		